國立臺灣大學生物資源暨農學院生物科技研究所

碩士論文

Institute of Biotechnology

College of Bioresources and Agriculture

National Taiwan University

Master's Thesis

HEN1 甲基化能力對於植物 RNA 靜默影響層次研究

Study on the impact of HEN1 methylation activities on RNA silencing mechanisms in *planta*

鍾昭慈

Chao-Tzu Chung

指導教授: 林詩舜 博士

Advisor: Shih-Shun Lin, Ph.D

中華民國 114 年 7 月

July, 2025

doi:10.6342/NTU202503912

國立臺灣大學碩士學位論文
口試委員會審定書

MASTER'S THESIS ACCEPTANCE CERTIFICATE
NATIONAL TAIWAN UNIVERSITY

HEN1 甲基化活性對於植物 RNA 靜默影響層次研究

Studying on the impact of HEN1 methylation activities on RNA silencing mechanisms in *planta*

本論文係 鍾昭慈 (姓名) R12642010 (學號) 在國立臺灣大學生物科技研究所 (系/所/學位學程)完成之碩士學位論文，於民國_114_年__7__月_25_日承下列考試委員審查通過及口試及格，特此證明。

The undersigned, appointed by the Department / Institute of Biotechnology on 25 (date) 7 (month) 114 (year) have examined a Master's thesis entitled above presented by Chao_Tzu Chung (name) R12642010 (student ID) candidate and hereby certify that it is worthy of acceptance.

口試委員 Oral examination committee:

林詩舜 (指導教授 Advisor)

陳荷明　邱子珍　劉力瑜

范木宗

系主任/所長 Director:

謝辭

在碩士研究的旅程即將告一段落之際，我心中滿懷感激，這一路上有歡笑也有疲憊，但沒有我身邊的貴人們出現，這個旅程不會如此的精彩。能有這個旅程，多虧了林詩舜教授，在沒有任何實驗經驗以及相關背景的我出現在您的面前，您不僅沒有嫌棄，反而看見我可以有更多可能性，還給我足夠的信任成為了管理實驗室帳務的重要工作，讓我如今能夠成為獨立完成研究的碩士生。

但在一開始，未知的知識如同海洋般浩瀚，管理帳務的工作又充滿需要注意的細節，對於懵懂無知的我，這兩座巨大的壓力使我喘不上氣，一度讓我心態崩潰，失去了繼續前行的動力，我能夠撐過那段艱苦的時光，多虧老師細心開導我，不停給我信心，有任何實驗上的困難，昭君學姊、育翎學姊、瑄斐學姊、薇倫學姊也會耐心的指導，同時我實驗室的夥伴陳亮合、鄭璇、余佳蓁、郭家齡也不停給我加油打氣。儘管當下的日子如同黑白，生命中的貴人們都在這段路幫我照亮了光，讓我在研究中不斷探索與精進。

同時也要感謝我的家人，尤其是父母和姊姊。所有辛苦與憂愁，回到家溫暖的懷抱就都會煙消雲散，有您們的支持與鼓勵是我堅持下去的最大動力。最後想再特別感謝我的同學與研究室的夥伴們，在我要去京都出差前的一週，需要有創新性的研究導致每天日以繼夜地做實驗，那時的你們不用我說就會想盡辦法想幫助我，有時甚至一起加班到晚上 11 點。儘管身體是如此的疲憊，但心靈真的非常富足，那是我非常寶貴且美好的回憶。每天一起相處、一起做實驗、一起在學術上交流，讓我這兩年的旅途多了許多溫暖與回憶。感謝所有在我求學路上曾經幫助過我的人，因為有您們的支持，我才能夠完成這段重要的旅程。未來，我將帶著這份感恩，繼續努力前行。

doi:10.6342/NTU202503912

中文摘要

RNA 靜默 (RNA silencing) 是調控基因表達的重要機制，主要透過小 RNA (如 siRNA 和 miRNA) 來調節目標 mRNA 的切割或翻譯抑制。HUA ENHANCER 1 (HEN1) 作為 2'-*O*-甲基轉移酶，負責對小 RNA 的 3' 端進行甲基化修飾，以保護其免受核酸酶降解並維持穩定性。當 HEN1 失去活性時會產生未甲基化的 miRNA，隨後 HESO1 會對其進行尿苷化修飾，使其降解。P1/HC-Pro^{Tu} 作為 RNA 靜默的病毒抑制子 (VSRs)，其功能會抑制 HEN1 結合 miRNA 的活性，進而影響 RNA 靜默機制。本研究探討了 HEN1 體外與體內甲基化活性對植物基因調控及 RNA 靜默能力的影響。我們成功構建了可誘導表達的 HESO1 轉基因植物 (*HA-HESO1/P1/HC-Pro^{Tu}/heso1*-1 和 *HESO1-HA/P1/HC-Pro^{Tu}/heso1-1*)，為進一步研究 HESO1 與 AGO1 相互作用奠定基礎。透過體外生化實驗證實， his-AtHEN1^{D719N} 完全失去甲基化 miRNA 的能力，直接證明了 D719N 突變對 RNA 靜默功能的關鍵影響。值得注意的是，地錢 (*Marchantia polymorpha*) MpHEN1 中相同保守位點的突變 (D760N) 仍保留部分甲基化活性，顯示不同物種間蛋白質功能演化的差異。轉錄組分析顯示，*hen1-8* 突變體和 P1/HC-Pro^{Tu} 在基因表達模式上表現出相似性。基因-基因網絡分析發現 76 個共同基因，其中 11 個基因與光信號傳導相關，包括生物鐘核心組件 CCA1 、 LHY 和 PRR5 等，進一步揭示 RNA silencing 可能與其他機制的相關性。降解組分析進一步揭示了 HEN1、HESO1 和 P1/HC-Pro^{Tu} 在調節 RNA 靜默中的複雜相互作用。本研究為理解 HEN1 甲基化活性在植物發育和環境適應中的分子機制提供了重要見解，且首次在體外實驗證實了 AtHEN1^{D719N} 的甲基化功能喪失，並藉由基因-基因網絡分析為 RNA 靜默機制的研究開闢了新方向。

關鍵詞：RNA 靜默, HEN1 甲基轉移酶, P1/HC-Pro^{Tu}, HESO1, 甲基化

doi:10.6342/NTU202503912

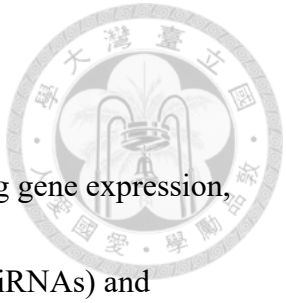

Abstract

RNA silencing is a crucial regulatory mechanism for controlling gene expression, primarily mediated by small RNAs such as short interfering RNAs (siRNAs) and microRNAs (miRNAs), which regulate target mRNA cleavage or translational repression. HUA ENHANCER 1 (HEN1), functioning as a 2'-*O*-methyltransferase, is responsible for methylating the 3' termini of small RNAs to protect them from nuclease degradation and maintain their stability. Loss of HEN1 activity results in the production of unmethylated miRNAs, which are subsequently uridylated by HESO1 and targeted for degradation. P1/HC-Pro^{Tu}, serving as a viral suppressor of RNA silencing (VSR), functions by inhibiting the methyltransferase (MTase) activity of HEN1 to bind miRNAs, thereby disrupting RNA silencing mechanisms.

This study examines the impact of HEN1 MTase activity, both *in vitro* and *in vivo,* on plant gene regulation and RNA silencing capacity. We successfully constructed inducible HESO1 transgenic plants (*HA-HESO1/P1/HC-Pro^{Tu}/heso1-1* and *HESO1-HA/P1/HC-Pro^{Tu}/heso1-1* plants) and established a foundation for further investigation of HESO1-mediated autophagic AGO1 degradation. Moreover, through *in vitro* methylation activity assay, we confirmed that his-AtHEN1^{D719N} (the mutant form of AtHEN1) completely loses its ability to methylate miRNAs, directly demonstrating the critical impact of the D719N mutation on RNA silencing function. Notably, the

doi:10.6342/NTU202503912

corresponding conserved site mutation (D760N) in *Marchantia polymorpha* HEN1 (MpHEN1) retains partial methylation activity, revealing evolutionary differences in protein function between species. Transcriptomic analysis revealed similarities in gene expression patterns between *hen1-8* mutant and *P1/HC-Pro*^{Tu} plants. Gene-to-gene network analysis identified 76 common genes, of which 11 are associated with light signaling pathways, including core circadian clock components *CCA1*, *LHY*, and *PRR5*. This further reveals potential correlations between RNA silencing and other regulatory mechanisms. Degradome analysis further elucidated the complex interactions among HEN1, HESO1, and P1/HC-Pro^{Tu} in the regulation of RNA silencing. This study offers valuable insights into the molecular mechanisms underlying HEN1 methylation activity in plant development and environmental adaptation. We present the first *in vitro* experimental evidence confirming the loss of methylation function in AtHEN1^{D719N} and establish new research directions for RNA silencing mechanisms through gene-to-gene network analysis.

Keywords: RNA silencing, HEN1, P1/HC-Pro^{Tu}, HESO1, Methylation

doi:10.6342/NTU202503912

Table of Contents

doi:10.6342/NTU202503912

doi:10.6342/NTU202503912

doi:10.6342/NTU202503912

List of figures

doi:10.6342/NTU202503912

doi:10.6342/NTU202503912

Introduction

RNA silencing is a crucial regulatory mechanism for gene expression. This mechanism primarily involves small RNAs, such as short interfering RNAs (siRNAs) and microRNAs (miRNAs), which can target their target mRNA, promote its degradation, or inhibit translation (Incarbone and Dunoyer, 2013). The RNA silencing pathway begins with the recognition of aberrant RNA structures, including double-stranded RNA (dsRNA), highly structured single-stranded RNA, or transgene-derived transcripts. These target RNAs are processed by DICER-LIKE (DCL) proteins, primarily DCL1, DCL2, DCL3, and DCL4, which cleave the dsRNA precursors into 21- to 24-nucleotide (nt) small RNA duplexes (Deleris et al., 2006). The resulting small RNA duplexes possess characteristic 2-nt 3' overhangs and 5' phosphate groups. Following DCL processing, the small RNA duplexes undergo strand selection, where one strand (guide strand) is preferentially loaded into RNA-induced silencing complexes (RISC). In contrast, the passenger strand is typically degraded. The incorporated guide strand directs RISC to target complementary mRNA sequences. Crucially, Hua Enhancer 1 (HEN1), a 2'-*O*-methyltransferase (MTase), plays a crucial role in the methylation of small RNA 3'-ends, which involves the addition of a methyl group to the 2'-OH of the 3'-terminal nucleotides of small RNA, resulting in methylated miRNAs (Met-miRNAs), which also protect them from 3' to 5' exonuclease degradation

doi:10.6342/NTU202503912

and ensure their stability (Yu et al., 2005). After HEN1 methylates siRNA or miRNA, these stabilized small RNAs are loaded into the RISC complex and bind to argonaute 1 (AGO1). The RISC then recognizes and binds to target mRNAs through sequence complementarity, ultimately executing gene silencing functions. MiRNAs primarily inhibit translation or promote mRNA degradation (Bartel, 2004; Guo et al., 2010).

The processing of Met-miRNA prevents miRNA degradation by nucleases, thereby stabilizing miRNAs. The full-length of *Arabidopsis* HEN1 (AtHEN1) is 942 amino acids. AtHEN1 has five domains, including two double-stranded RNA binding domains (dsRBD1 and dsRBD2), La-motif-containing domain (LCD), PPIase-like domain (PLD), and MTase domain (Huang et al., 2009). Current studies demonstrate that the *hen1-8* mutant of *Arabidopsis* exhibits a series of phenotypes (Chen et al., 2002; Yu et al., 2005). The *hen1-8* plant of *Arabidopsis* has the D719N mutation on the MTase of HEN1. These phenotypes clearly confirm the critical role of HEN1 in normal plant growth and development. However, current research on *hen1-8* mutant phenotypes primarily relies on *in vivo* genetic analysis and phenotypic observations, lacking direct biochemical evidence to elucidate how HEN1 lose its activity to regulate these developmental processes at the molecular level.

Marchantia polymorpha, commonly known as liverwort, belongs to the bryophytes, an early land plant. Previous studies have indicated that the HEN1 of plant

doi:10.6342/NTU202503912

species share a common ancestor and exhibit highly conserved sequence identities, especially in the MTase domain. Moreover, *M. polymorpha* HEN1 (MpHEN1) contains the same functional domains as AtHEN1 (Sanobar et al., 2021). Currently, *M. polymorpha* has become one of the most studied model plants. However, research on *M. polymorpha* RNA silencing is limited, mainly because *M. polymorpha* is haploid, and the majority of RNA silencing component genes, such as MpHEN1 and MpAGO1, are critical and exist in a single copy (Pietrykowska et al., 2022). Once these genes mutate, it directly leads to lethality, making it impossible to produce viable mutant strains.

The P1/helper-component protease (P1/HC-Pro) from turnip mosaic virus (TuMV) is a viral suppressor of RNA silencing (VSR) (Kasschau et al., 2003). Yu et al. (2006) demonstrated that the miRNA methylation is inhibited in transgenic *Arabidopsis* expressing the HC-Pro gene of TuMV. Pan et al. (2025) further confirmed that HC-Pro^{Tu} counteracts RNA silencing by inhibiting HEN1 from methylating miRNA, resulting in unmethylated miRNAs (unMet-miRNAs), and leading to the autophagic degradation of AGO1. When AGO1 is degraded by autophagy, the amount of RISC decreases, leading to a reduction in RNA silencing efficiency.

When AGO1-bound miRNAs accomplish their functional roles and require metabolic degradation, A family of DEDD 3' to 5' exonucleases known as small RNA degrading nucleases (SDNs) step in to initiate the degradation process by first removing

doi:10.6342/NTU202503912

the methyl group from the miRNA 3'-ends (Chen et al., 2018). Following demethylation, HEN1 suppressor factor 1 (HESO1), a terminal uridylyl transferase (TUTase), adds uridines to miRNA (Tu et al., 2015). This uridylation serves as a signal for the degradation of the miRNA. Pan et al. (2025) observed the presence of unmethylated miRNA and the restoration of AGO1 levels in *P1/HC-Pro^{Tu}/hen1-8/heso1-1* plants, suggesting that HESO1 may trigger the autophagic degradation of AGO1 during the loading of unmethylated miRNA. However, the complex relationships among P1/HC-Pro^{Tu}, HEN1, HESO1, and AGO1 still require further research.

In light of recent findings, we propose four key questions: (1) Does HESO1 reduce AGO1 protein levels? (2) Does the D719N mutation in the AtHEN1 recombinant protein possess methylation activity? Does MpHEN1, which carries a mutation at the same conserved site, retain methylation capability? (3) Are there differentially expressed genes in *hen1-8* mutants and *P1/HC-Pro^{Tu}* plants that influence regulatory mechanisms other than RNA silencing? (4) What are the effects on RNA silencing in the double mutant *hen1-8/heso1-1* plants, the *P1/HC-Pro^{Tu}/heso1-1* plants, and the *P1/HC-Pro^{Tu}/hen1-8/heso1-1* plants?

In this study, we successfully induced the HESO1 transgene in the *P1/HC-Pro^{Tu}/heso1-1* background, and the relationship between HESO1 and AGO1 can be further explored in the future. Furthermore, we employed *in vitro* experiments to

doi:10.6342/NTU202503912

demonstrate that His-AtHEN1^{D719N} has lost the ability to methylate miRNAs, directly proving that His-AtHEN1^{D719N} affects RNA silencing. Notably, the mutation at the same conserved site of MpHEN1 retained the partial methylation activity, highlighting the protein differences between species. Since *hen1-8* mutants and *P1/HC-Pro^{Tu}* plants both generate unMet-miRNAs, we performed transcriptomic analysis with gene-to-gene network modeling. This comparative approach revealed similarities between the *hen1-8* mutant and the *P1/HC-Pro^{Tu}* plants, paving the way for a new direction in investigating RNA silencing mechanisms.

doi:10.6342/NTU202503912

Materials and methods

Plant material and growth conditions

Arabidopsis thaliana Columbia (Col-0), *hen1-8/heso1-1*, *P1/HC-Pro^{Tu}/heso1-1, P1/HC-Pro^{Tu}/hen1-8/heso1-1* plants (Pan et al., 2024), *HA-HESO1/P1/HC-Pro^{Tu}/heso1-1*, *HESO1-HA/P1/HC-Pro^{Tu}/heso1-1* plants were used in this study. The seeds were surface-sterilized with 70% ethanol and 3% bleach containing 0.01% Tween-20 before germinating on half-strength MS (0.9% agar, pH 5.7) medium or MS media, both them supplemented with or without the appropriate antibiotics. All plants were incubated in a growth room (24 h light, 22-24℃). Seven-day-old seedling of *HA-HESO1/P1/HC-Pro^{Tu}/heso1-1* and *HESO1-HA/P1/HC-Pro^{Tu}/heso1-1* were transferred to MS media with or without the bestradiol inducer and maintained under 24 h light at 22-24℃ for seven days.

Purification of recombinant protein

Protein expression constructs of pET28a-his-AtHEN1, pET28a-his-AtHEN1^{D719N}, pET28a-his-MpHEN1, and pET28a-his-MpHEN1^{D760N} plasmids were introduced into Escherichia coli Rosetta BL21 strain, then propagated on Luria Agar (LA) medium containing the appropriate antibiotics for 16 h. A single colony was inoculated in 10 mL Luria Broth (LB) with the antibiotics for 16 h at 37℃, 220 rpm.

doi:10.6342/NTU202503912

Subsequently, the culture was diluted into LB medium at a 1:100 (v/v) ratio and maintained at 37℃ with agitation at 150 rpm. The bacteria were chilled at 19℃ with agitation at 150 rpm for 30 min, followed by the addition of IPTG to a final concentration of 0.1 mM to trigger protein expression, and then maintained at 19℃ with agitation at 90 rpm for 16-20 h. Afterwards, the cells were collected by centrifugation at 4,000-5,000 rpm for 10 min at 4℃, then suspended in 60-100 mL of lysis buffer (50 mM Tris-HCl, pH 8.0, 300 mM NaCl, 1 mM DTT, and 10 mM imidazole) supplemented with newly prepared 1 mM phenylmethylsulfonyl fluoride (PMSF). The cells were disrupted at 15,000-18,000 psi using a high-pressure cell disrupter until the solution became transparent. The cell lysate was centrifuged at 13,000 rpm for 30 min at 4℃, and the supernatant was passed through a 0.45 μm filter. The filtered sample was loaded onto a HisTrap column. The column was washed with wash buffer (50 mM Tris-HCl, pH 8.0, 300 mM NaCl, 1 mM DTT, and 20 mM imidazole), and the bound proteins were recovered using elution buffer (50 mM Tris-HCl, pH 8.0, 300 mM NaCl, 1 mM DTT, and 200 mM imidazole). The eluted fractions were examined via SDS-PAGE, and the purified proteins were dialyzed overnight at 4℃ in dialysis buffer (10 mM Tris-HCl, pH 8.0, 100 mM NaCl, 1 mM DTT, 0.1 mM EDTA, and 2 mM MgCl2) at a 1:100 (v/v) ratio. The dialyzed proteins were preserved at 4℃.

doi:10.6342/NTU202503912

Western blot

The protein solution was mixed with an equal volume of 2× SDS loading buffer (2% SDS, 10% glycerol, 1% β-mercaptoethanol, 0.05% bromophenol blue, and 50 mM Tris-HCl pH 6.8). Subjected to 100℃ for 5-10 min and chilled on ice for 5 min. 10-15 μL of each specimen was applied onto SDS-PAGE for examination. The gel was blotted onto a PVDF membrane using migration buffer (50 mM Tris-base, 40 mM glycine, 1 mM SDS, and 20% methanol). The membrane was masked in rinse buffer containing 5% skim milk for 1 h at ambient temperature and maintained overnight at 4℃ with the primary antibody. The following day, the membrane was rinsed and maintained for 1 h at ambient temperature with HRP-linked anti-rabbit IgG. After rinsing, the membrane was visualized using the WesternBright ECL system. Results were measured with Image J's gel analysis function.

HEN1 activity assay

The synthetic miR159 sense and antisense strands were annealed using 5× annealing buffer (300 mM KCl, 30 mM HEPES pH 7.5, and 1 mM $MgCl_2$) at 95℃ for 5 min and then cooled down gradually to room temperature. A total of 0.4 ng of ds-syn-miR159 was then subjected to a methylation process with different content of purified proteins (his-AtHEN1, his-AtHEN1^{D719N}, his-MpHEN1, and his-MpHEN1^{D760N}), 10 μL

doi:10.6342/NTU202503912

NEB Cutsmart buffer with 0.01 μL DTT, and 3.2 mM SAM. The solution was incubated at 37℃ for 90-120 min.

β-elimination

The periodate oxidation method was employed to examine methylation activity of HEN1. The isolated RNA was mixed in 176 μL of 0.06M borax/boric acid (pH 8.6) and 24 μL of newly prepared 0.2 M sodium periodate, followed by reaction in darkness at room temperature for 1 h. The mixture was filtered through the pre-packed Sephadex G-25 resin (GE Healthcare). One-tenth volume of glycerol was subsequently added, followed by an additional 30-min reaction period. The mixture was precipitated with 1 μL of glycogen (15μg/μL), 22 μL of 3 M NaOAc, and 800 μL of 99% EtOH. The solution was spun at 13,000 rpm, 4℃, for 15 min after being kept on ice for 10 min. After RNA precipitation, β-elimination was conducted with 100 μL of 0.055M borax/boric acid/NaOH (pH 9.5) at 45℃ for 90 min. The mixture was then purified with Sephadex G-25 resin. Finally, the RNA was precipitated once more and analyzed using small RNA northern blot analysis.

Northern blot

In northern blot analysis, the FA dye was added to the RNA samples at a 1:1 ratio,

doi:10.6342/NTU202503912

and the mixture was incubated at 65℃ for 10 min. The sample was then cooled on ice for 5 min. The RNA samples were separated on a 20% polyacrylamide gel with 8 M urea. After running gel electrophoresis in 1× TBE buffer, the gel was transferred to a Hybond-N+ membrane by a Semi-Dry transfer system. The cross-linked membrane was prehybridized with Ambion Ultrahyb-Oligo solution at 42℃ for 1 h. Afterward, the membrane was hybridized with γ-32P labeled antisense miR159. The X-ray film exposed the miR159 signals on the membrane at -80℃. The results were quantified using the gel analysis function in ImageJ.

Electrophoretic mobility shift assay (EMSA)

The artificial complementary sequences of miR159 and miR160a were paired in 5× coupling buffer (30 mM HEPES pH 7.5, 300 mM KCl, and 1 mM MgCl2) at 95℃ for 5 min. Subsequently, the temperature was slowly reduced to ambient temperature. The ds-syn-miR159 and ds-syn-miR160a were γ-32P-tagged using T4 polynucleotide kinase and cleaned with G-25 beads. Isolated proteins were combined with 0.4 ng of γ-32P-tagged ds-syn-miR159 solution with reaction mixture (5×; 40 mM Tris-HCl, pH 8.0, 1 mM MgCl2, 30 mM KCl, 0.01% NP-40, and 1 mM dithiothreitol). The solution was maintained for 1 h at ambient temperature. Following incubation, the reaction was blended with 6× loading buffer (0.25% bromophenol blue, 0.25% xylene cyanol, and

doi:10.6342/NTU202503912

40% glycerol) and applied onto a 5% native gel (30% acrylamide 37.5:1, 0.5× TBE buffer, 10% APS, and 1% TEMED). Electrophoresis was conducted at 60V for 1 h. The gel was dehydrated at 60℃ for 45 min, then subjected to X-ray film at -20℃.

Degradome library construction and sequencing

Degradome analysis was performed to assess the expression levels of miRNA-targeted mRNAs by analyzing the RISC 3'-cleavage fragments, following the protocol by Hong et al. (2024). Total RNA was extracted from 14-day-old plant seedlings using the Plant Total RNA Extraction Miniprep Kit (Viogene-Biotek Corporation, New Taipei City, Taiwan). A total of 10 μg of extracted RNA was used to isolate mRNA using the Dynabeads mRNA DIRECT Purification Kit (Thermo Fisher Scientific). To further purify the mRNA, the eluted mRNA was repurified using Dynabeads. After isolation, the RNA was heated to 70°C and ligated with a 5' adaptor (12 μM) using T4 RNA ligase 1 (New England Biolabs) at 25°C for 2 h. The ligated mRNA was then purified again using Dynabeads to remove any excess 5' adaptors. The purified 5' ligated RNA was precipitated with isopropanol (Honeywell) and glycoblue (Thermo Fisher Scientific) at -80°C for 12 h to concentrate the samples. The precipitated mRNA was subjected to reverse transcription using a 3' adaptor random primer (20 μM) and a poly(T) primer (2.6 μM) with the SuperScript IV Reverse Transcriptase kit (Thermo Fisher Scientific).

doi:10.6342/NTU202503912

The resulting cDNA library was amplified via PCR using a forward primer and a unique reverse primer (250 nM) each containing a 6-nt index for sequencing identification using the LongAmp Taq 2× Master Mix kit (New England Biolabs) for 15 to 17 cycles. The amplified cDNA library was purified using Agencourt AMPure XP beads (Beckman-Coulter). Finally, cDNA concentration and fragment distribution were measured using the Qubit dsDNA HS Assay Kit (Thermo Fisher Scientific) and QSep1 (Bioptic). Sequencing was performed on the NovaSeq X platform (Illumina) in paired-end mode with a read length of 150 bp. The degradome analysis was conducted as described by Lin et al. (2016).

Whole-transcriptome analysis

The transcriptome analysis was conducted using the ContigViews platform (www.contigviews.bioagri.ntu.edu.tw), developed by the Next-Generation Sequencing Core Facility at National Taiwan University, which specializes in transcriptomic data visualization and network analysis. For the network analysis performed in this study, differentially expressed genes (DEGs) with a twofold change in expression levels among Col-0, hen1-8, and P1/HC-Pro^{Tu} samples (n = 3) and an 80% success rate across biological replicates were selected. To minimize background noise from low-expression genes, genes with $\log_{10}$ FPKM values below 1.14 were excluded. Pearson correlation

doi:10.6342/NTU202503912

coefficients were calculated to evaluate the interactions between gene expression levels, with a cutoff of 0.92 for positive correlations and -0.92 for negative correlations. Parameter selection was based on the expression levels and biological significance of prominent genes while considering the complexity of the network structure to optimize data exploration. The gene interaction network was constructed and visualized using the ContigViews platform, where node size and edge thickness represent the importance of genes and the strength of interactions, respectively.

doi:10.6342/NTU202503912

Results

Inducible *HA-HESO1/P1/HC-Pro^{Tu}/heso1-1* and *HESO1-HA/P1/HC-Pro^{Tu}/heso1-1* plants

We aim to generate inducible HESO1 transgenic constructs, which are incorporated in *P1/HC-Pro^{Tu}/heso1-1* plant background. To achieve this purpose, we conducted two inducible *HESO1* constructs, *HA-HESO1* and *HESO1-HA* genes, driven by pER8 binary vector, named pER8-HA-HESO1 and pER8-HESO1-HA, respectively (Fig.1A). Both inducible binary vectors were transferred into *P1/HC-Pro^{Tu}/heso1-1* plant by agrobacterium-mediated flowering transformation.

To confirm AtHESO1 expression, we first performed Agrobacterium-mediated transient transformation in *Nicotiana benthamiana* leaves with AtHESO1-YFP and YFP control constructs (Fig. 1B). We obtained an *HA-HESO1/P1/HC-Pro^{Tu}/heso1-1* plant line #6, which has a HA-tag fusion at the N-terminal of HESO1 (Fig. 1A, panel i). In addition, we obtained another line, *HESO1-HA/P1/HC-Pro^{Tu}/heso1-1* plants line #7, which has a HA-tag fusion at the C-terminal of HESO1 (Fig. 1A, panel ii). Both lines were capable of being induced by β-estradiol inducer to generate HA-HESO1 and HESO1-HA (Fig. 1C, panel i). Western blot analysis revealed that *HA-HESO1/P1/HC-Pro^{Tu}/heso1-1* plants induced HA-HESO1, approximately 66 kDa by β-estradiol treatment; whereas *HESO1-HA/P1/HC-Pro^{Tu}/heso1-1* plants induced HESO1-HA,

doi:10.6342/NTU202503912

approximately 64 kDa (Fig. 1C, panel i). Quantitative analysis showed that HA-HESO1 expression was 2.38-fold higher than HESO1-HA expression (Fig. 1C, panel ii). Notably, transient-expressed AtHESO1-YFP showed at 75 kDa, which was used as HESO1 positive control (Fig. 1C, panel i). Neither the mock treatment of *N. Benthamiana* nor Col-0 plants exhibited undetectable HESO1 (Fig. 1C, panel i), thereby both transgenic HESO1 plants in *P1/HC-Pro*^{Tu}*/heso1-1* background has been confirmed successful inducting HESO1. The results of the failure to detect the endogenous HESO1 in Col-0 plants may be due to the low levels of endogenous HESO1 that are out of the detection limit of the a-HESO1 antibody. To investigate whether HESO1 affects AGO1 levels, we used Actin as an internal reference gene for normalization and quantified AGO1 expression levels relative to Actin loading. HA-HESO1 induction showed increased AGO1 levels; however, the Actin loading in this sample differed substantially from other samples, making it difficult to establish a clear correlation. In contrast, HESO1-HA induction showed a decreasing trend in AGO1 levels compared to the control group (Fig. 1C, panel ii).

D719 of HEN1 is a conserved amino acid in the MTase domain

We compared the AtHEN1 amino acid sequences of Arabidopsis (AtHEN1), which belongs to angiosperms, and *Marchantia polymorpha* (MpHEN1), which belongs

doi:10.6342/NTU202503912

to bryophytes (Fig. 2). The sequence alignment between AtHEN1 and MpHEN1 revealed a 54% similarity, suggesting potential functional similarities. Yu et al. (2010) demonstrated that the *hen1-8* mutant, which has a D719N mutation on the MTase of AtHEN1, affects the MTase activity. The D719 residue on the MTase of AtHEN1 is a highly conserved amino acid, whereas MpHEN1, it is also conserved at position 760 (D760). We suggested that D760 in MpHEN1 might also play a critical role in the activity of MTase.

Although the *hen1-8* mutant has been shown to have the unMet-miRNA *in vivo* (Zhao et al., 2012), there is no evidence that any AtHEN1^{D719N} methylation activity has been demonstrated *in vitro*. Therefore, we would like to demonstrate recombinant His-AtHEN1^{D719N} methyltransferase activity *in vitro*. Additionally, we aim to create a recombinant MpHEN1^{D760N} to assess the methyltransferase activity in this study.

Construction and purification of the HEN1 recombinant protein

To investigate how the functionality of the *hen1-8* mutant is altered, we used the pET28a-his-AtHEN1 plasmid as a template and employed site-directed mutagenesis to generate the his-AtHEN1^{D719N} in the pET28a vector, named pET28a-his-AtHEN1^{D719N} (Fig. 3). We employed *E. coli* to express pET28a-his-AtHEN1 and pET28a-his-AtHEN1^{D719N}. We utilized FPLC for purification of these recombinant proteins (Fig. 4).

doi:10.6342/NTU202503912

Given that only one amino acid was modified, the a-AtHEN1 antibody retained its ability to recognize his-AtHEN1^{D719N} (Fig. 5). Western blot analysis indicated that we successfully purified the his-AtHEN1 (130 kDa) and his-AtHEN1^{D719N} (130 kDa).

Based on our successful expression of the his-AtHEN1^{D719N} in bacteria, we aim to purify his-MpHEN1^{D760N} to investigate the MpHEN1 MTase activity. Therefore, we collaborated with a laboratory at Kyoto University and obtained the his-MpHEN1^{D760N} for the *in vitro* activity evaluation. his-AtHEN1, his-AtHEN1^{D719N}, his-MpHEN1, and his-MpHEN1^{D760N} were purified by His-Trap column. The solubilized his-HEN1 showed a 130 kDa band in the eluted fractions (Fig. 4). The purified proteins can be subjected to functional assays *in vitro*.

Small RNA binding of AtHEN1 is not affected by the D719N mutation in the MTase domain

First, we aimed to examine how the stability of his-AtHEN1 and his-AtHEN1^{D719N} affects their activity. To assess this, we purified two batches of his-AtHEN1 and his-AtHEN1^{D719N} at different time points. One batch was stored at 4°C for 6 weeks, while the other batch was stored at 4°C for 3 weeks. We utilized electrophoretic mobility shift assays (EMSA) to evaluate the binding capability of his-AtHEN1 and his-AtHEN1^{D719N} to miRNA duplex. The EMSA results indicated that his-AtHEN1 and his-AtHEN1^{D719N},

doi:10.6342/NTU202503912

stored for 6 weeks, lost their ability to bind miRNA duplexes, whereas the proteins stored for 3 weeks retained the ability to bind most miRNA duplexes (Fig. 6A). These results indicate that the stability of his-AtHEN1 and his-AtHEN1^{D719N} is critical for *in vitro* experiments.

Next, we aimed to demonstrate that his-AtHEN1^{D719N} retains the capacity to bind small RNAs. We separately used miR159 duplex and miR160a duplex with his-AtHEN1 and his-AtHEN1^{D719N}. The EMSA results showed that both his-AtHEN1 and his-AtHEN1^{D719N} retained the ability to bind miRNA duplexes (Fig. 6B and C). These findings suggested that the D719N mutation on the MTase of AtHEN1 does not affect small RNA binding.

D719N on MTase domain of AtHEN1 affects MTase activity

We demonstrated that the ability of his-AtHEN1^{D719N} in binding small RNAs. Next, we aimed to determine whether his-AtHEN1^{D719N} retains the ability to methylate the small RNAs. The β-elimination-treated miRNAs revealed methylated miR159 (Met-miR159), where the band was present at the 21-nt positions, while unmethylated miR159 (unMet-miR159) showed at the 20-nt positions (Fig. 7A). Quantitative results of three biological replicates indicate that his-AtHEN1 exhibited an average of 55% Met-miR159 and 45% unMet-miR159 (Fig. 7A and B). In contrast, his-AtHEN1^{D719N}

doi:10.6342/NTU202503912

displayed 100% unMet-miR159 (Fig. 7A and B). These findings demonstrated that his-AtHEN1^{D719N} has lost the ability to methylate miRNAs. This indicates that the D719N mutation in the MTase of AtHEN1 affects its methylation capability.

In principle, the *in vitro* his-HEN1 activity assay should show most Met-miRNA. However, the his-AtHEN1 only showed an average 55% Met-miR159 (Fig. 7). Therefore, we aim to develop several approaches to reduce the proportion of unMet-miRNA. The first approach was to re-anneal the miR160a duplex. Before performing the HEN1 activity assay, we incubate the miR160a duplex at 50°C for 1 min, then allow it to cool to room temperature slowly. The result of the re-annealing miR160a duplex reacted with his-AtHEN1 showed 64% and 51% Met-miR160a (Fig. 8A). The non-reannealed miR160a duplex reacted with his-AtHEN1 showed 52% and 59% Met-miR160a (Fig. 8A). The data suggested that the reannealed miR160a duplex might solve the unMet-miRNA problem in his-HEN1 activity assay.

Next, we increased the dose of his-AtHEN1 in the *in vitro* assay. The results showed that the dose of his-AtHEN1 was 0.3 ng, with a Met-miRNA ratio of 34% (Fig. 8B). However, increasing the dose of his-AtHEN1 to 0.6 ng resulted in a Met-miRNA ratio of 59%. Moreover, the dose of his-AtHEN1 was 1.8 ng and showed that 79% Met-miRNAs (Fig. 8B). These findings indicated that the dose of his-AtHEN1 affects the amount of methylation of small RNAs, and reannealing miRNA duplexes is a necessary

doi:10.6342/NTU202503912

step before performing the *in vitro* HEN1 activity assay.

His-MpHEN1^{D760N} retained its methylation capability

We also aimed to investigate his-MpHEN1^{D760N} to evaluate its MTase activity. First, we utilized EMSA to evaluate the small RNA binding activity of his-MpHEN1 and his-MpHEN1^{D760N}. We incubated the miR159 duplex with his-MpHEN1 and his-MpHEN1^{D760N}. The results indicated that both his-MpHEN1 and his-MpHEN1^{D760N} can bind with the miR159 duplexes (Fig. 9A), which is consistent with the findings observed for his-AtHEN1 and his-AtHEN1^{D719N}.

Furthermore, we aimed to determine whether his-MpHEN1^{D760N} retains the ability to methylate small RNAs. The β-elimination results revealed that negative control (miR159 duplexes) appeared as a 100% of 21-nt Met-miR159, and 0% of 20-nt unMet-miR159 (Fig. 9B). Quantitative analysis indicated that the methylation activity of his-MpHEN1 increased in a dose-dependent manner with the amount of recombinant protein present (Fig. 9B). The dose of his-MpHEN1 as 0.55 ng, the results showed 67% Met-miR159 and 33% unMet-miR159 (Fig. 9B). And increasing the dose of his-MpHEN1 as 1.1 ng, the result showed that 100% Met-miR159. In contrast, 0.62ng of his-MpHEN1^{D760N} showed 38% Met-miR159 and 62% unMet-miR159 (Fig. 9B). Interestingly, 3.1 ng of his-MpHEN1^{D760N} showed 46% Met-miR159 and 54% unMet-

doi:10.6342/NTU202503912

miR159 (Fig. 9B). These results revealed that his-MpHEN1 is capable of miRNA methylation. However, his-MpHEN1^{D760N} still retains partial MTase activity, unlike his-AtHEN1^{D719N}, which has completely lost the MTase capability.

Comparative gene-to-gene network and transcriptome analysis

In previous studies, comparative network analysis of P1/HC-Pro^{Tu} revealed an overall perspective to identify many critical genes involved in RNA silencing (Hu et al., 2020). P1/HC-Pro^{Tu} suppresses HEN1 to produce unMet-miRNA, while the *hen1-8* mutant loss-of-function mutation also generates unMet-miRNA. This prompted us to further explore whether the gene networks resulting from these two conditions are similar. The comparative analyses of the RNA-Seq profiles of Col-0 vs. P1/HC-Pro^{Tu}, sample, and Col-0 vs. *hen1-8* sample sets revealed 1990 and 1454 DEGs, respectively. These DEGs were then used for a network analysis using the ContigViews system, which revealed 247 and 170 genes in the networks, respectively (Fig. 10A). A Venn diagram showed that 76 genes were found in both comparative analyses (Fig. 10B).

To further elucidate the functions of the common genes in the *P1/HC-Pro^{Tu}* plants and *hen1-8* mutants, we performed gene annotation and functional classification. Among these 76 common genes, 11 genes are indicated to be related to light signaling. *CIRCADIAN CLOCK ASSOCIATED 1* (*CCA1*), *LATE ELONGATED HYPOCOTYL*

doi:10.6342/NTU202503912

(*LHY*), and *PSEUDO-RESPONSE REGULATOR 5* (*PRR5*) are core components of the biological clock that affect plant growth and development by regulating the circadian rhythm (Alabadí et al., 2002; Nakamichi et al., 2012). *CCA1* and *LHY* were positively correlated and *PRR5* is located in negatively correlated regions (Fig. 11). Siré et al. (2009) pointed out that changes in miRNA accumulation throughout the day appear to be a response to light and are not governed by the circadian clock. This finding provides a valuable perspective for investigating whether genes related to the circadian clock, such as *CCA1* and *LHY*, may have other regulatory effects. The molecular mechanism by which CCA1 influences the circadian expression of *GRP7* and its significance for clock output—specifically, pathogen defense—has been emphasized important defense gene in plants (Gao et al., 2022).

CONSTANS-LIKE 2 (*COL2*), *FLAVIN-BINDING KELCH REPEAT F-BOX 1* (*FKF1*), *CYCLING DOF FACTOR 3* (*CDF3*), *CYCLING DOF FACTOR 5* (*CDF5*), and *SALT TOLERANCE HOMOLOGUE* (*STH*) participate in light signal perception and transduction (Imaizumi et al., 2003; Gangappa et al., 2013; Corrales et al., 2017; Zhang et al., 2023). *CDF3* was shown to be positively correlated with *CCA1* and *COL2*, and *STH* (Fig. 11). *PRR5* and *CDF5* are located in negatively correlated regions. *HY5 HOMOLOG (HYH)*, *GOLDEN2-LIKE 2* (*GLK2*), and *HOMEOBOX PROTEIN 23* (*HB23*) are involved in the transcriptional regulation of light-signaling response (Choi

doi:10.6342/NTU202503912

et al., 2014; Marzi et al., 2020; Zhang et al., 2024). *GLK2* is positively correlated with *STH, COL2,* and *HYH* (Fig. 11). *HB23* is related to genes such as *GLUTATHIONE S-TRANSFERASE F8* (*GSTF8*) and *HIGH MOBILITY GROUP B2* (*HMGB2*), which respond to environmental changes. These 11 light-signaling miRNA target transcripts were downregulated in *hen1-8* mutants and *P1/HC-Pro*^{Tu} plants compared to Col-0 plants (Fig. 12A-K).

Next, we focused on 9 genes responsive to environmental changes. *NUCLEOBASE-CATION SYMPORTER 1* (*NCS1*), *CYSTEINE PROTEINASE 1* (*CP1*), and *ABSCISIC ACID RESPONSIVE ELEMENTS-BINDING FACTOR 1* (*ABF1*) are positively correlated with light signaling genes and were downregulated in *hen1-8* mutants and *P1/HC-Pro*^{Tu} plants compared to Col-0 plants. *UDP-GLYCOSYLTRANSFERASE 72E1* (*UGT72E1*) is positively correlated with *ERBB-3 BINDING PROTEIN* (*EBP*), and *FIONA 4* (*FIN4*). *FIN4* is positively correlated with *NCS1* and *CP1. NAC DOMAIN CONTAINING PROTEIN 83* (*NAC083*) is positively correlated with *HMGB2* and *SERINE ACETYLTRANSFERASE 32* (*SAT32*). *HMGB2* is positively correlated with *HB23* and negatively correlated with *GSTF8.* These 9 miRNA target transcripts that respond to environmental changes were downregulated in *hen1-8* mutants and *P1/HC-Pro*^{Tu} plants compared to Col-0 plants (Fig. 13A-I).

Finally, we focused on the other 5 genes responsive to environmental changes.

doi:10.6342/NTU202503912

FLOWERING LOCUS R1 (*FLOR1*) is negatively correlated with *COL2, CP1* and *UGT72E1. GLYCOSYL HYDROLASE 9B13* (*GH9B13*) is negatively correlated with *UGT72E1*. *ARABINOGALACTAN PROTEIN 18* (*AGP18*) is positively correlated with *GSTF8*, which is responsible for regulating the selection and survival of plant cells (Demesa-Arévalo and Vielle-Calzada, 2013b). *GSTF8* is an important gene in plant defense responses (Dixon et al., 2002), which is negatively correlated with *HMGB2* and *HB23*. HMGB2, as a high mobility group protein, participates in chromatin remodeling and transcriptional regulation (Pedersen and Grasser, 2010). Its downregulation may compromise the plant's transcriptional response capacity to environmental stresses. *LIPOXYGENASE 2* (*LOX2*) regulates the expression of defense genes by synthesizing signaling molecules such as Jasmonic acid (Bell et al., 1995; Wasternack and Song, 2016). These 5 miRNA target transcripts that respond to environmental changes were upregulated in *hen1-8* mutants and *P1/HC-Pro*^{Tu} plants compared to Col-0 plants (Fig. 14A-E).

The *hen1-8* mutants and *P1/HC-Pro*^{Tu} plants exhibited similar transcript expression patterns, providing important insights into understanding the role of plant RNA silencing mechanisms in regulating light signal transduction and environmental adaptation.

Due to the presence of numerous distinct genes in the networks of *hen1-8* and

doi:10.6342/NTU202503912

P1/HC-Pro^{Tu}, after analyzing the common genes shared between *hen1-8* and P1/HC-Pro^{Tu}, we further focused on the gene-to-gene interaction network unique to Col-0 vs *hen-8* network. We observed that *AGP18* appears among the common genes; however, it exhibits significant negative correlations with several unique genes of Col-0 vs *hen-8* network (Fig.11). AGP18 plays a critical role in the structure and stability of the cell wall (Demesa-Arévalo and Vielle-Calzada, 2013a). Interestingly, *AGP18* shows a positive correlation with *RAPID ALKALINIZATION FACTOR 22* (*RALFL22*), a gene known to regulate plant growth, development, and immune responses (Morcillo et al., 2024). We investigated the transcript expression of genes related to AGP18 and RALFL22, and found that the transcript expression patterns of these genes differed between *hen1-8* and P1/HC-Pro^{Tu} plants (Fig. 15). Based on these findings, we propose that the differences between the networks of *hen1-8* and P1/HC-Pro^{Tu} may, in part, involve the regulation of genes affecting cell wall stability.

Degradome analysis of Col-0, *hen1-8/heso1-1, P1/HC-Pro^{Tu}/heso1-1,* and *P1/HC-Pro^{Tu}/hen1-8/heso1-1* plants

According to Zhao et al. (2012) findings, the *heso1-1* mutation can partially rescue the developmental and molecular defects of *hen1-8* plants. To further explore the effects of interactions between these genes on RNA silencing. We used degradome

doi:10.6342/NTU202503912

sequencing to detect RNA-specific cleavage and miRNA-mediated cleavage. We analyzed Col-0, *hen1-8/heso1-1*, *P1/HC-Pro^{Tu}/heso1-1*, and *P1/HC-Pro^{Tu}/hen1-8/heso1-1* plants to focus on degradome variations of the RISC cleavage fragments for the miRNA target genes.

Compared with Col-0 plants, the *hen1-8/heso1-1* mutants exhibited an increase in RISC cleavage fragments for some miRNA target genes, including AGO2, GRF1 etc. (Fig 16 and 17). In addition, the degradome reads of *ARF16*, *SPL6*, and *NAC2* decreased. In contrast, both *P1/HC-Pro^{Tu}/heso1-1* and *P1/HC-Pro^{Tu}/hen1-8/heso1-1* plants showed a general decrease in RISC cleavage fragments for most miRNA target genes, with the exceptions of *MYB65*, *SPL3*, and *GRF1*, which exhibited increased cleavage fragments in their respective results (Fig. 16). Furthermore, *ARF16, SPL6,* and *NAC2* showed decreased cleavage fragments in all mutants compared with Col-0 plants, while *AGO2, GRF3, MYB65,* and *SPL3* showed an increase in RISC 5' cleavage fragments only in *hen1-8/heso1-1* plants (Fig. 18). These results indicate that the *hen1-8/heso1-1* mutation disrupts miRNA homeostasis, leading to selective changes in RISC cleavage activity rather than general functional restoration. In contrast, the expression of P1/HC-Pro^{Tu} generally inhibits miRNA-mediated cleavage, with exceptions in certain genes. This reflects the high complexity of the RNA silencing regulatory mechanism.

doi:10.6342/NTU202503912

Discussion

Transgenic HESO1 successes were induced in *P1/HC-Pro^{Tu}/heso1-1* plants

In this study, under the *P1/HC-Pro^{Tu}/heso1-1* background, we successfully induced the expression of HA-HESO1 or HESO1-HA (Fig.1C). With β-estradiol induction, the HESO1-HA was induced while the AGO1 protein content showed a decrease in *HESO1-HA/P1/HC-Pro^{Tu}/heso1-1* plants. Pan et al. (2025) demonstrated that HC-Pro^{Tu} inhibits HEN1 activity and triggers the autophagic degradation of AGO1, which is triggered by HESO1 when unMet-miRNAs are loaded onto AGO1. Further experiments are needed to clarify the relationship between HESO1 expression and AGO1 levels through more consistent dose-response studies. To be able to demonstrate that HESO1 reduces AGO1 levels.

In future studies, we can adjust the timing of β-estradiol induction, the concentration of β-estradiol, or consider that HESO1 may have been induced at an earlier time, such as during seed germination. Also, in the *P1/HC-Pro^{Tu}/heso1-1* background, the transgene of *P1/HC-Pro^{Tu}* was driven by the constitutive expression of the CaMV 35S promoter, which is active throughout seed development. However, due to the *heso1-1* mutation, HESO1-mediated degradation of AtAGO1 does not occur, resulting in continuous accumulation of AtAGO1. Additionally, AtAGO1 protein may have a relatively slow degradation rate, making AtAGO1 difficult to observe significant

doi:10.6342/NTU202503912

changes within a short induction period.

Another experiment, which we can try, will treat the plants with the cycloheximide (CHX) to block new AtAGO1 synthesis after b-estradiol induction and monitor AGO1 levels over time to determine protein half-life. Moreover, HESO1 induced in both transgenic plants was only seven days, which may not have been sufficient to impact the stability or degradation of AGO1 significantly. In future studies, the effect of HESO1 on AGO1 degradation could be further investigated by varying the duration of induction or by altering the developmental stage at which induction is initiated.

Species-specific effects of conserved HEN1 point mutations on RNA methylation activity

This study confirmed that the his-AtHEN1^{D719N} completely loses the ability to methylate miRNAs *in vitro* (Fig. 7A), consistent with previous *in vivo* observations of *hen1-8* mutant (Yu et al., 2010). This demonstrates that D719 in AtHEN1, as the key catalytic amino acid in the MTase domain, is essential for maintaining methyl transfer activity. Interestingly, although the D760 in MpHEN1 occurs at the corresponding conserved position, it only partially loses its methyl transfer activity (Fig. 9B). Based on the amino acid sequences of AtHEN1 and MpHEN1, we found that the protein sequence

doi:10.6342/NTU202503912

similarity between AtHEN1 and MpHEN1 is 54%. In comparison, the similarity of their MTase domains is only 42%, suggesting that even highly conserved catalytic sites can still be influenced by the overall protein structure and the evolutionary context of the species.

These findings have important implications for understanding the evolution and adaptability of RNA silencing mechanisms, and also suggest that *M. polymorpha* may possess higher functional redundancy or mechanistic flexibility. Currently, there are very few studies on MpHEN1. To further understand the role of RNA silencing in *M. polymorpha*, we can knock out the *hen1* gene and introduce the Mp*hen1*^{D760N} gene, thereby generating Mp*HEN1*^{D760N}/Mp*hen1*^{ge} mutant lines. These transgenic and mutant plants will provide a valuable platform for investigating the role of RNA silencing in the development of antheridia in *M. polymorpha*.

Evaluation of HEN1 activity and the significance of reannealing miRNA duplexes

This study employed three variables to improve HEN1 *in vitro* experiments: (1) re-annealed versus non-re-annealed miRNA, (2) HEN1 content dosage, and (3) HEN1 with different storage durations. The experiments confirmed that miRNA duplex re-annealing, HEN1 content, and HEN1 stability all influence experimental outcomes. This study also demonstrated that his-AtHEN1 completely lost its miRNA binding activity

doi:10.6342/NTU202503912

after six weeks of storage at 4°C (Fig. 6A), indicating that protein stability is crucial for *in vitro* experiments. Furthermore, we utilized EMSA to detect the ability of HEN1 to bind small RNAs, suggesting that EMSA can be employed to assess HEN1 activity prior to conducting future HEN1 *in vitro* experiments. Biotechnology companies previously commercialized HEN1 but may have discontinued sales due to storage difficulties. Yu et al. (2005) stored purified HEN1 at -80°C. In our study, we used purified HEN1 within three weeks under 4°C storage conditions for experiments. In future studies, we can evaluate different storage methods for purified HEN1 to ensure its stability and avoid compromising the interpretation of experimental results.

Network reveals *hen1-8* mutants and *P1/HC-Pro^{Tu}* plants association with light signaling

In the gene-to-gene network, *hen1-8* mutants and *P1/HC-Pro^{Tu}* plants share 76 common genes, among which 26 genes exhibit similar miRNA target transcript expression patterns (Fig. 12, 13, and 14). According to the study by Tsai et al. (2014), HEN1 is a negative regulator of photomorphogenesis and is closely associated with the expression of photoreceptors (such as *PHYA*, *PHYB*, *CRY1*, and *CRY2*) and key transcription factors HY5 and HYH. Notably, *HYH* is also among these 76 common genes, further supporting the association between HEN1 and the light signaling

doi:10.6342/NTU202503912

mechanism. Based on the similarity in miRNA target transcript expression patterns of the common genes between *hen1-8* mutants and *P1/HC-Pro*^{Tu} plants, we propose a hypothesis suggesting that RNA silencing may be related to light signaling (Fig.19). The plant circadian clock and light signaling systems form a complex regulatory network through RNA silencing mechanisms. Under normal conditions, core clock genes CCA1 and LHY are expressed in the morning and directly suppress PRR5 transcription. PRR5 protein accumulates in the afternoon and provides negative feedback to inhibit CCA1 and LHY, creating circadian oscillations. This clock system regulates downstream photomorphogenesis genes (*HY5*, *HYH*) and flowering time regulators (*FKF1, CDF3, CDF5, COL2*). Crucially, HY5 and HYH activate HEN1, promoting miRNA methylation. Met-miR157d can cleave its target mRNA, providing negative feedback regulation of HY5 to maintain system balance (Fig. 19A). This precise regulatory mechanism ensures plants can appropriately respond to light signals while maintaining normal physiological rhythms. When the RNA silencing system is disrupted, plant light signaling becomes abnormal. In *hen1-8* mutants, HEN1 loses its methylation function, causing unMet-miRNAs to become unstable. These unmethylated miRNAs are uridylated by HESO1 and subsequently degraded. Similarly, P1/HC-Pro^{Tu} inhibits HEN1 methylation activity, producing the same result. Due to the degradation of miR157d, the negative feedback regulation of HY5 is lost, leading to HY5

doi:10.6342/NTU202503912

overexpression (Fig. 19B). This regulatory imbalance may disrupt the entire light signaling network, affecting plant photomorphogenesis, flowering time regulation, and the maintenance of circadian rhythms. This hypothesis requires further investigation to validate these observations.

Unlike the Col-0_HC network, the Col-0_hen1-8 network contains only a few genes that may be indirectly involved in RNA silencing, such as *RNE* and *DOF5*, whose specific roles require further investigation. Additionally, appropriately adjusting the parameter settings for correlation thresholds during the construction of expressional correlational networks may help to explore these genes more comprehensively.

Our degradome analysis revealed the complex interactions among HEN1, HESO1, and P1/HC-Pro^{Tu} in regulating RNA silencing. Degradome reads represent the number of 5' fragments generated from mRNA cleavage by the miRNA-guided RISC complex, detected through sequencing. The loss-of-function *hen1-8* mutation results in unMet-miRNAs being uridylated by HESO1 and subsequently degraded, leading to reduced miRNA levels and impaired RNA silencing regulation. The *hen1-8/heso1-1* double mutant exhibits partial restoration of miRNA function, as evidenced by the increased RISC cleavage fragments of specific target genes such as AGO2 and GRF1. These findings are consistent with findings of Zhao et al. (2012), which showed that the *hen1-8/heso1-1* phenotype is partially restored to normal. Pan et al. (2025) observed that in

doi:10.6342/NTU202503912

P1/HC-Pro^{Tu}*/hen1-8/heso1-1* plants, unMet-miRNAs are present, and AGO1 levels are restored. However, our data show that only GRF1 exhibits increased RISC cleavage fragments in *P1/HC-Pro*^{Tu}*/hen1-8/heso1-1* plants. Due to the lack of replicates and control groups, these observations require further studies to clarify unknown mechanisms. Future studies incorporating degradome analyses of *hen1-8, heso1-1*, and P1/HC-Pro^{Tu} will enable more precise comparisons of RISC-mediated cleavage patterns.

doi:10.6342/NTU202503912

Conclusion

Through *in vitro* biochemical assays, we successfully demonstrated that the D719N mutation in AtHEN1 completely lost its MTase activity, providing direct biochemical evidence for the critical role of this conserved amino acid residue. Interestingly, the corresponding mutation (D760N) in MpHEN1 retained partial methylation activity, revealing evolutionary divergence in protein function between different plant species. We constructed inducible HESO1 transgenic plants, although whether HESO1 can reduce AGO1 levels remains to be investigated. Transcriptomic analysis revealed striking similarities between *hen1-8* mutants and *P1/HC-Pro*^{Tu} plants, with gene network analysis identifying 76 common genes, including many light-signaling-related genes. This discovery unveils the connection between RNA silencing and light-responsive pathways. Our degradome analysis further elucidated the intricate regulatory network involving HEN1, HESO1, and P1/HC-Pro^{Tu} in RNA silencing. These findings not only advance our fundamental understanding of RNA silencing mechanisms but also provide new perspectives on the evolutionary conservation and functional diversification of HEN1 across plant species.

doi:10.6342/NTU202503912

Reference

Alabadí, D., Yanovsky, M.J., Más, P., Harmer, S.L., and Kay, S.A. (2002). Critical role for CCA1 and LHY in maintaining circadian rhythmicity in Arabidopsis. Curr Biol **12,** 757-761.

Bartel, D.P. (2004). MicroRNAs: genomics, biogenesis, mechanism, and function. Cell **116,** 281-297.

Bell, E., Creelman, R.A., and Mullet, J.E. (1995). A chloroplast lipoxygenase is required for wound-induced jasmonic acid accumulation in Arabidopsis. Proceedings of the National Academy of Sciences **92,** 8675-8679.

Chen, J., Liu, L., You, C., Gu, J., Ruan, W., Zhang, L., Gan, J., Cao, C., Huang, Y., Chen, X., and Ma, J. (2018). Structural and biochemical insights into small RNA 3′ end trimming by Arabidopsis SDN1. Nature Communications **9,** 3585.

Chen, X., Liu, J., Cheng, Y., and Jia, D. (2002). HEN1 functions pleiotropically in Arabidopsis development and acts in C function in the flower. Development **129,** 1085-1094.

Choi, H., Jeong, S., Kim, D.S., Na, H.J., Ryu, J.S., Lee, S.S., Nam, H.G., Lim, P.O., and Woo, H.R. (2014). The homeodomain-leucine zipper ATHB23, a phytochrome B-interacting protein, is important for phytochrome B-mediated red light signaling. Physiol Plant **150,** 308-320.

doi:10.6342/NTU202503912

Corrales, A.R., Carrillo, L., Lasierra, P., Nebauer, S.G., Dominguez-Figueroa, J., Renau-Morata, B., Pollmann, S., Granell, A., Molina, R.V., Vicente-Carbajosa, J., and Medina, J. (2017). Multifaceted role of cycling DOF factor 3 (CDF3) in the regulation of flowering time and abiotic stress responses in Arabidopsis. Plant Cell Environ **40,** 748-764.

Deleris, A., Gallego-Bartolome, J., Bao, J., Kasschau, K.D., Carrington, J.C., and Voinnet, O. (2006). Hierarchical Action and Inhibition of Plant Dicer-Like Proteins in Antiviral Defense. Science **313,** 68-71.

Demesa-Arévalo, E., and Vielle-Calzada, J.-P. (2013a). The Classical Arabinogalactan Protein AGP18 Mediates Megaspore Selection in Arabidopsis The Plant Cell **25,** 1274-1287.

Demesa-Arévalo, E., and Vielle-Calzada, J.P. (2013b). The classical arabinogalactan protein AGP18 mediates megaspore selection in Arabidopsis. Plant Cell **25,** 1274-1287.

Dixon, D.P., Davis, B.G., and Edwards, R. (2002). Functional divergence in the glutathione transferase superfamily in plants. Identification of two classes with putative functions in redox homeostasis in *Arabidopsis thaliana*. J Biol Chem **277,** 30859-30869.

Gangappa, S.N., Crocco, C.D., Johansson, H., Datta, S., Hettiarachchi, C., Holm,

doi:10.6342/NTU202503912

M., and Botto, J.F. (2013). The Arabidopsis B-BOX protein BBX25 interacts with HY5, negatively regulating BBX22 expression to suppress seedling photomorphogenesis. Plant Cell **25,** 1243-1257.

Gao, M., Zhang, C., Angel, W., Kwak, O., Allison, J., Wiratan, L., Hallworth, A., Wolf, J., and Lu, H. (2022). Circadian regulation of the GLYCINE-RICH RNA-BINDING PROTEIN gene by the master clock protein CIRCADIAN CLOCK-ASSOCIATED 1 is important for plant innate immunity. Journal of Experimental Botany **74,** 991-1003.

Guo, H., Ingolia, N.T., Weissman, J.S., and Bartel, D.P. (2010). Mammalian microRNAs predominantly act to decrease target mRNA levels. Nature **466,** 835-840.

Hu, S.-F., Wei, W.-L., Hong, S.-F., Fang, R.-Y., Wu, H.-Y., Lin, P.-C., Sanobar, N., Wang, H.-P., Sulistio, M., Wu, C.-T., Lo, H.-F., and Lin, S.-S. (2020). Investigation of the effects of P1 on HC-pro-mediated gene silencing suppression through genetics and omics approaches. Botanical Studies **61,** 22.

Huang, Y., Ji, L., Huang, Q., Vassylyev, D.G., Chen, X., and Ma, J.-B. (2009). Structural insights into mechanisms of the small RNA methyltransferase HEN1. Nature **461,** 823-827.

Imaizumi, T., Tran, H.G., Swartz, T.E., Briggs, W.R., and Kay, S.A. (2003). FKF1 is

doi:10.6342/NTU202503912

essential for photoperiodic-specific light signalling in Arabidopsis. Nature **426,** 302-306.

Incarbone, M., and Dunoyer, P. (2013). RNA silencing and its suppression: novel insights from in planta analyses. Trends Plant Sci **18,** 382-392.

Kasschau, K.D., Xie, Z., Allen, E., Llave, C., Chapman, E.J., Krizan, K.A., and Carrington, J.C. (2003). P1/HC-Pro, a viral suppressor of RNA silencing, interferes with Arabidopsis development and miRNA unction. Dev Cell **4,** 205-217.

Marzi, D., Brunetti, P., Mele, G., Napoli, N., Calò, L., Spaziani, E., Matsui, M., De Panfilis, S., Costantino, P., Serino, G., and Cardarelli, M. (2020). Light controls stamen elongation via cryptochromes, phytochromes and COP1 through HY5 and HYH. Plant J **103,** 379-394.

Morcillo, R.J.L., Leal-López, J., Férez-Gómez, A., López-Serrano, L., Baroja-Fernández, E., Gámez-Arcas, S., Tortosa, G., López, L.E., Estevez, J.M., Doblas, V.G., Frías-España, L., García-Pedrajas, M.D., Sarmiento-Villamil, J., and Pozueta-Romero, J. (2024). RAPID ALKALINIZATION FACTOR 22 is a key modulator of the root hair growth responses to fungal ethylene emissions in Arabidopsis. Plant Physiol **196,** 2890-2904.

Nakamichi, N., Kiba, T., Kamioka, M., Suzuki, T., Yamashino, T., Higashiyama, T.,

doi:10.6342/NTU202503912

Sakakibara, H., and Mizuno, T. (2012). Transcriptional repressor PRR5 directly regulates clock-output pathways. Proceedings of the National Academy of Sciences **109,** 17123-17128.

Pan, Z.-J., Wei, W.-L., Tran, P.-A., Fang, R.-Y., Pham, T.H., Bowman, J.L., Chung, C.-T., Shen, B.-N., Yang, J.-T., Chang, H.-H., Jane, W.-N., Cheng, C.-H., Wang, C.-C., Wu, H.-Y., Hong, S.-F., Shang, Q.-W., Hu, S.-F., Lin, P.-C., Wu, F.-H., Lin, C.-S., Hung, Y.-L., Shen, T.-L., and Lin, S.-S. (2025). HC-Pro inhibits HEN1 methyltransferase activity, leading to autophagic degradation of AGO1. Nature Communications **16,** 2503.

Pedersen, D.S., and Grasser, K.D. (2010). The role of chromosomal HMGB proteins in plants. Biochim Biophys Acta **1799,** 171-174.

Pietrykowska, H., Sierocka, I., Zielezinski, A., Alisha, A., Carrasco-Sanchez, J.C., Jarmolowski, A., Karlowski, W.M., and Szweykowska-Kulinska, Z. (2022). Biogenesis, conservation, and function of miRNA in liverworts. Journal of Experimental Botany **73,** 4528-4545.

Sanobar, N., Lin, P.C., Pan, Z.J., Fang, R.Y., Tjita, V., Chen, F.F., Wang, H.C., Tsai, H.L., Wu, S.H., Shen, T.L., Chen, Y.H., and Lin, S.S. (2021). Investigating the Viral Suppressor HC-Pro Inhibiting Small RNA Methylation through Functional Comparison of HEN1 in Angiosperm and Bryophyte. Viruses **13**.

doi:10.6342/NTU202503912

Siré, C., Moreno, A.B., Garcia-Chapa, M., López-Moya, J.J., and Segundo, B.S. (2009). Diurnal oscillation in the accumulation of Arabidopsis microRNAs, miR167, miR168, miR171 and miR398. Febs Letters **583,** 1039-1044.

Tsai, H.-L., Li, Y.-H., Hsieh, W.-P., Lin, M.-C., Ahn, J.H., and Wu, S.-H. (2014). HUA ENHANCER1 Is Involved in Posttranscriptional Regulation of Positive and Negative Regulators in Arabidopsis Photomorphogenesis The Plant Cell **26,** 2858-2872.

Tu, B., Liu, L., Xu, C., Zhai, J., Li, S., Lopez, M.A., Zhao, Y., Yu, Y., Ramachandran, V., Ren, G., Yu, B., Li, S., Meyers, B.C., Mo, B., and Chen, X. (2015). Distinct and cooperative activities of HESO1 and URT1 nucleotidyl transferases in microRNA turnover in Arabidopsis. PLoS Genet **11,** e1005119.

Wasternack, C., and Song, S. (2016). Jasmonates: biosynthesis, metabolism, and signaling by proteins activating and repressing transcription. Journal of Experimental Botany **68,** 1303-1321.

Yu, B., Chapman, E.J., Yang, Z., Carrington, J.C., and Chen, X. (2006). Transgenically expressed viral RNA silencing suppressors interfere with microRNA methylation in Arabidopsis. FEBS Letters **580,** 3117-3120.

Yu, B., Yang, Z., Li, J., Minakhina, S., Yang, M., Padgett, R.W., Steward, R., and Chen, X. (2005). Methylation as a crucial step in plant microRNA biogenesis.

doi:10.6342/NTU202503912

Science **307,** 932-935.

Yu, B., Bi, L., Zhai, J., Agarwal, M., Li, S., Wu, Q., Ding, S.W., Meyers, B.C., Vaucheret, H., and Chen, X. (2010). siRNAs compete with miRNAs for methylation by HEN1 in Arabidopsis. Nucleic Acids Res **38,** 5844-5850.

Zhang, B., Feng, M., Zhang, J., and Song, Z. (2023). Involvement of CONSTANS-like Proteins in Plant Flowering and Abiotic Stress Response. Int J Mol Sci **24**.

Zhang, T., Zhang, R., Zeng, X.-Y., Lee, S., Ye, L.-H., Tian, S.-L., Zhang, Y.-J., Busch, W., Zhou, W.-B., Zhu, X.-G., and Wang, P. (2024). GLK transcription factors accompany ELONGATED HYPOCOTYL5 to orchestrate light-induced seedling development in Arabidopsis. Plant Physiology **194,** 2400-2421.

Zhao, Y., Yu, Y., Zhai, J., Ramachandran, V., Dinh, Thanh T., Meyers, Blake C., Mo, B., and Chen, X. (2012). The Arabidopsis Nucleotidyl Transferase HESO1 Uridylates Unmethylated Small RNAs to Trigger Their Degradation. Current Biology **22,** 689-694.

doi:10.6342/NTU202503912

Figures

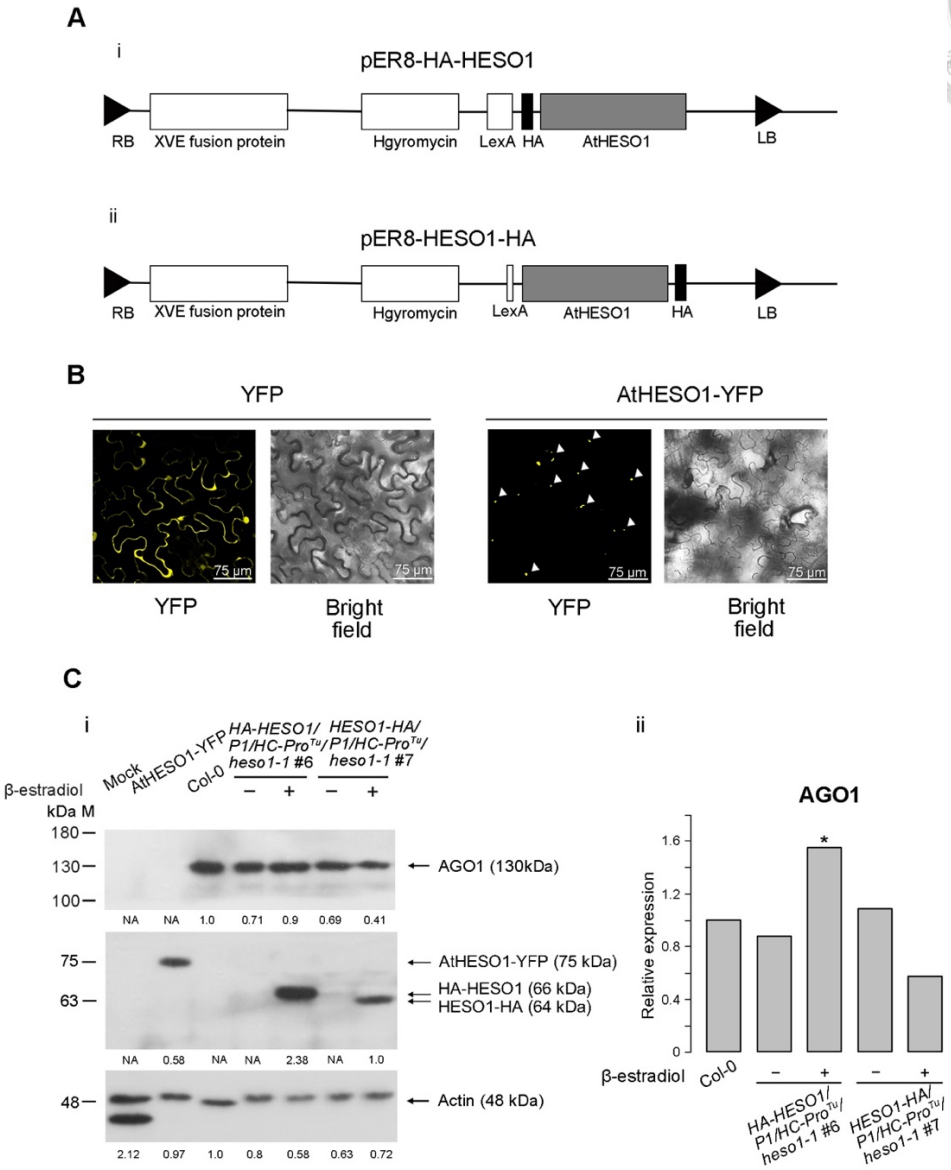

Figure 1. Detect HESO1 and AGO1 by western blot in *HA-HESO1/P1/HC-ProTu/heso1-1* and *HESO1-HA/P1/HC-ProTu/heso1-1*. (A)The schematic binary of pER8-HA-HESO1 (i) and pER8-HESO1-HA (ii). (B)The subcellular localization of YFP or AtHESO1-YFP, Bar, 75 μm. (C) Detection of AGO1, HESO1, and Actin from mock and AtHESO1-YFP in *N. benthamiana* and Col-0, *HA-HESO1/P1/HC-Pro^{Tu}/heso1-1*, and *HESO1-HA/P1/HC-Pro^{Tu}/heso1-1* in *Arabidopsis thaliana* (i). Quantification of AGO1 levels in Col-0 plants and mutants by bar chart, * indicates unexpected differences (ii).

doi:10.6342/NTU202503912

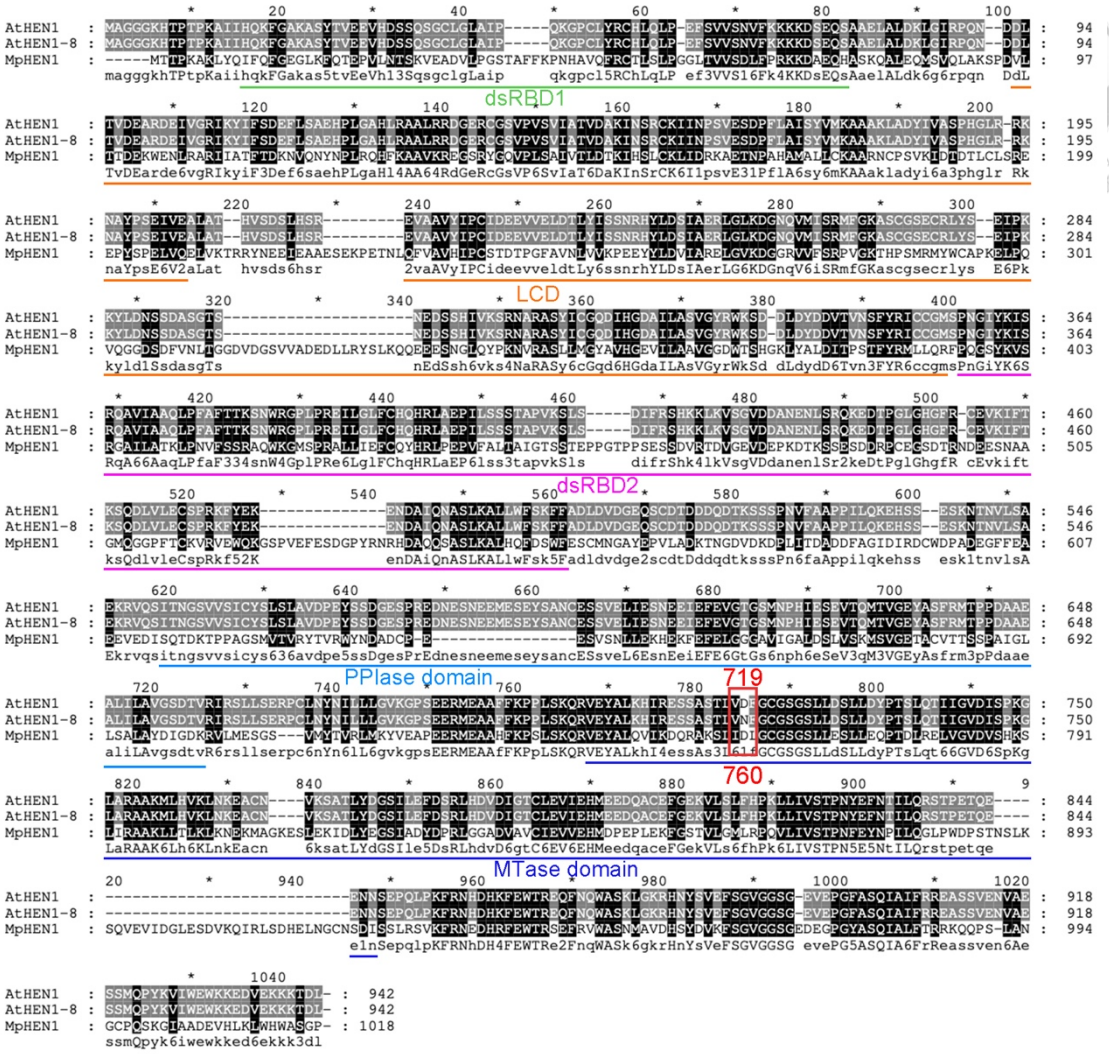

Figure 2. Comparing the amino acids sequence of AtHEN1, *hen1-8*, and MpHEN1 in *A. thaliana* and *M. polymorpha*. The results of AtHEN1, *hen1-8*, and MpHEN1 amino acid alignment. Amino acid sequence alignment for AtHEN1 and MpHEN1. The five domains are highlighted by a box based on AtHEN1 structure studies. The red box indicated the D719 of AtHEN1, N719 of *hen1-8*, and D760 of MpHEN1.

doi:10.6342/NTU202503912

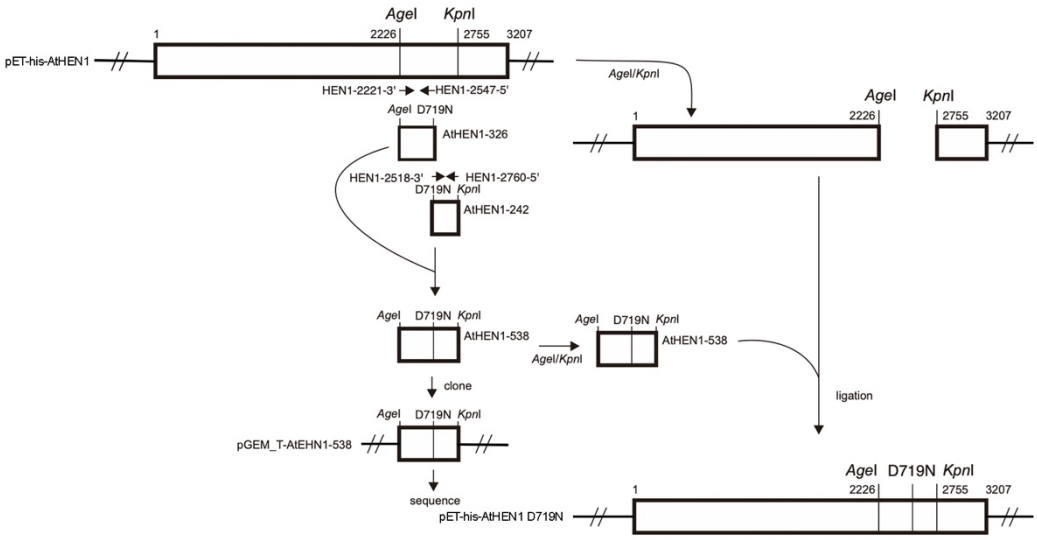

Figure 3. Construction of the his-AtHEN1^{D719N}. The pET-his-AtHEN1^{D719N} was constructed from a pET-his-AtHEN1.

doi:10.6342/NTU202503912

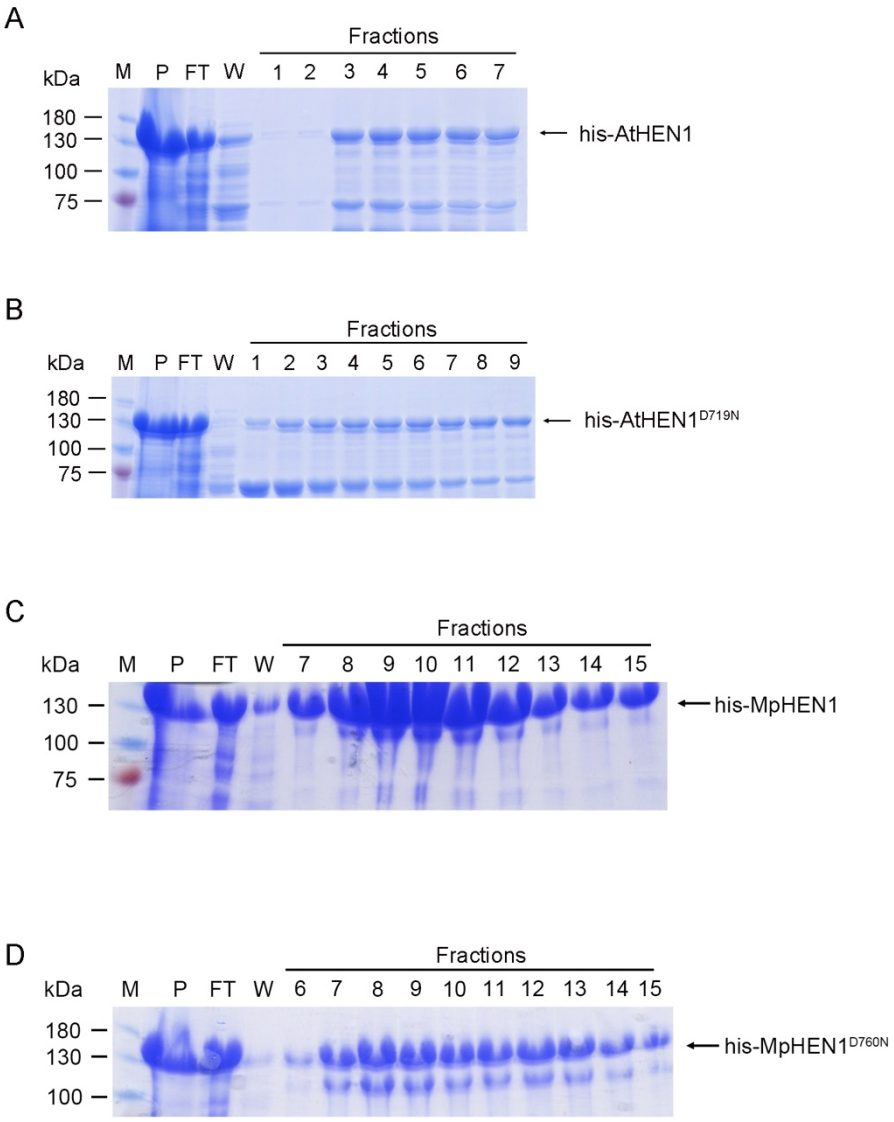

Figure 4. Recombinant proteins purification. (A) Purification of his-AtHEN1. (B) Purification of his-AtHEN1^{D719N}. (C) Purification of his-MpHEN1. (D) Purification of his-MpHEN1^{D760N}. M represents marker; P represents pellet; FT represents flow through; W represents wash. The numbers indicate the number of fractionation tubes.

doi:10.6342/NTU202503912

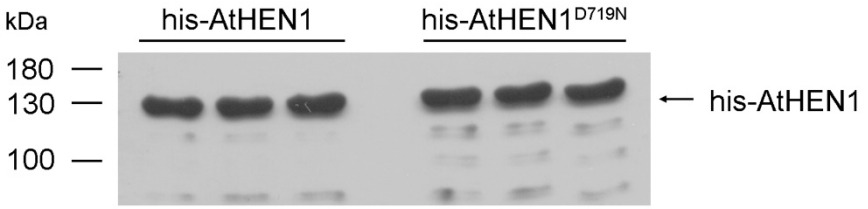

Figure 5. Detection of his-AtHEN1 and his-AtHEN1^{D719N} *in vitro*. His-AtHEN1 and his-AtHEN1^{D719N} recombinant protein were detected by his-AtHEN1 antibody with Western blot.

doi:10.6342/NTU202503912

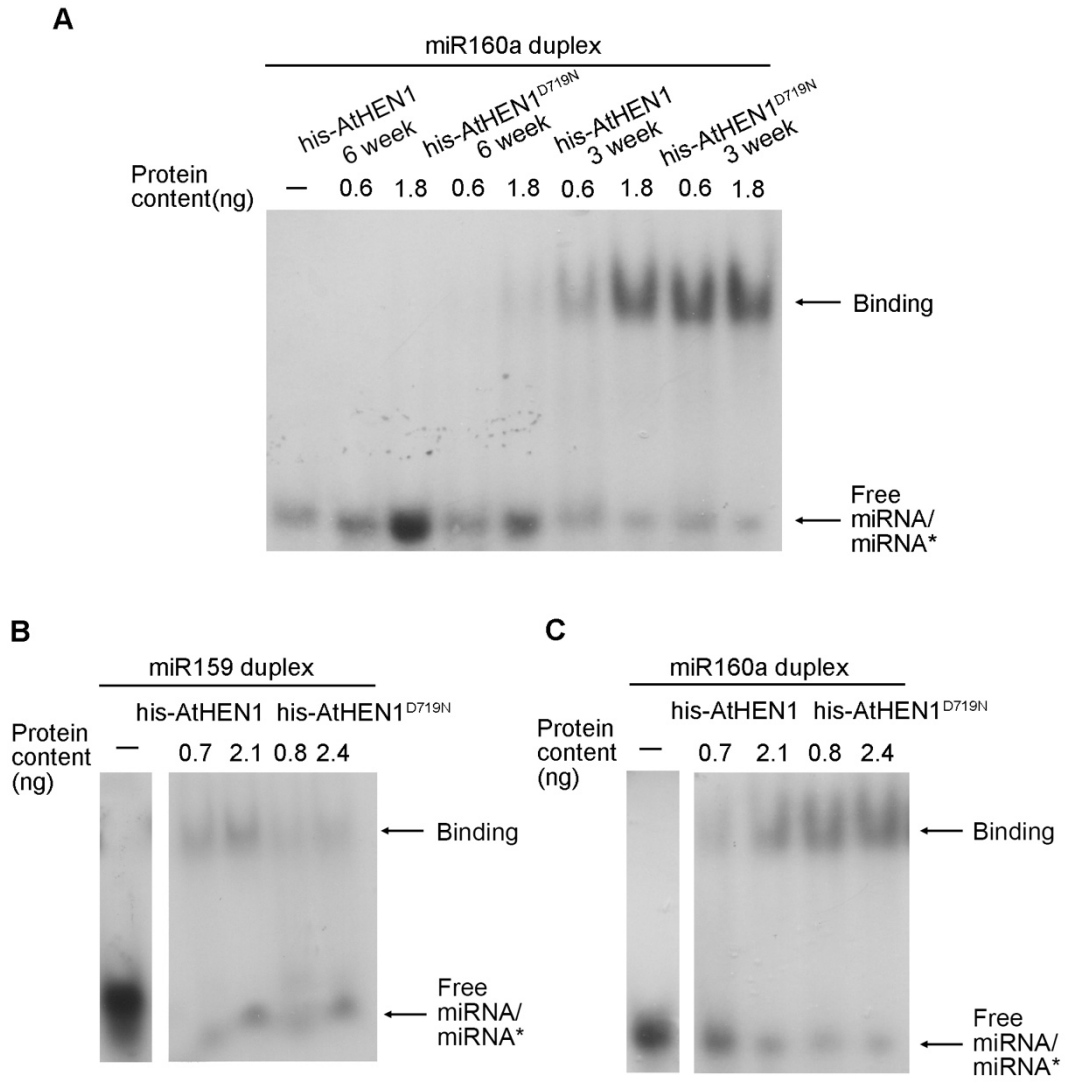

Figure 6. Evaluation for miRNA/miRNA* duplex binding activity of his-AtHEN1 and his-AtHEN1^{D719N}. (A) Compares the ability of binding miRNA for his-AtHEN1 and his-AtHEN1^{D719N} 6 weeks versus 3 weeks. The 0.4 ng of radioisotope-labeled double-stranded synthetic miRNA was used. *In vitro* EMSA for his-AtHEN1 and his-AtHEN1^{D719N} binding to miR159 duplexes (B) and miR160a duplexes (C).

doi:10.6342/NTU202503912

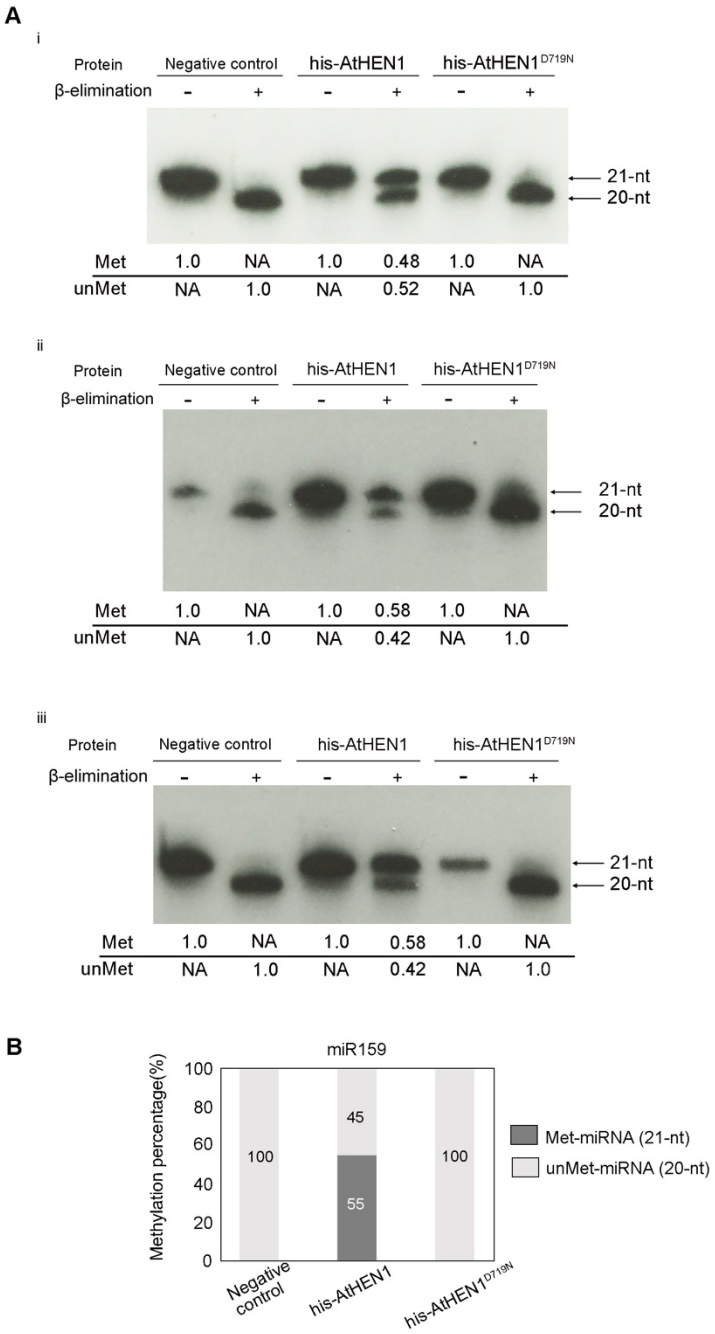

Figure 7. Evaluation of miRNA methylation status in his-AtHEN1 and his-AtHEN1D719N by β-elimination. (A) miRNA samples were treated with β-elimination (+) or without treatment (−). The 0.4 ng of radioisotope-labeled double-stranded synthetic miR159 without any protein was used negative control. The panels (i to iii) represent the results of three independent experiments. (B) Bar charts represent the percentage of methylated (Met) and unmethylated (unMet) miR159 in the samples.

doi:10.6342/NTU202503912

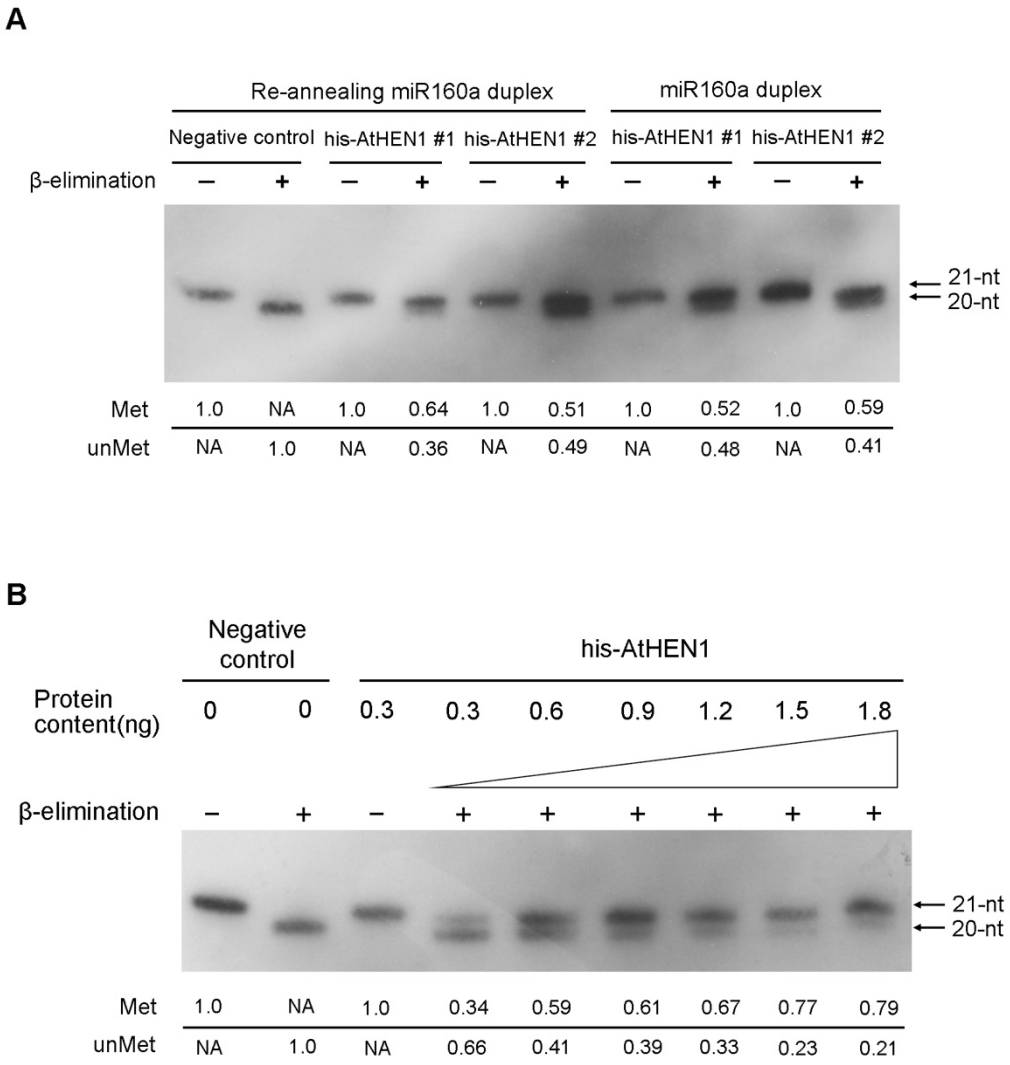

Figure 8. Evaluation of miRNA methylation status in his-AtHEN1. (A) The miR160a duplex with re-annealing or without re-annealing reacted with his-AtHEN1. (B) The re-annealing miR160a duplex reacted with different doses of his-AtHEN1. The 0.4 ng of radioisotope-labeled double-stranded synthetic miR160a without any protein was used negative control. Negative control consisted of 0.4 ng of radioisotope-labeled double-stranded synthetic miR159 or miR160a without any protein.

doi:10.6342/NTU202503912

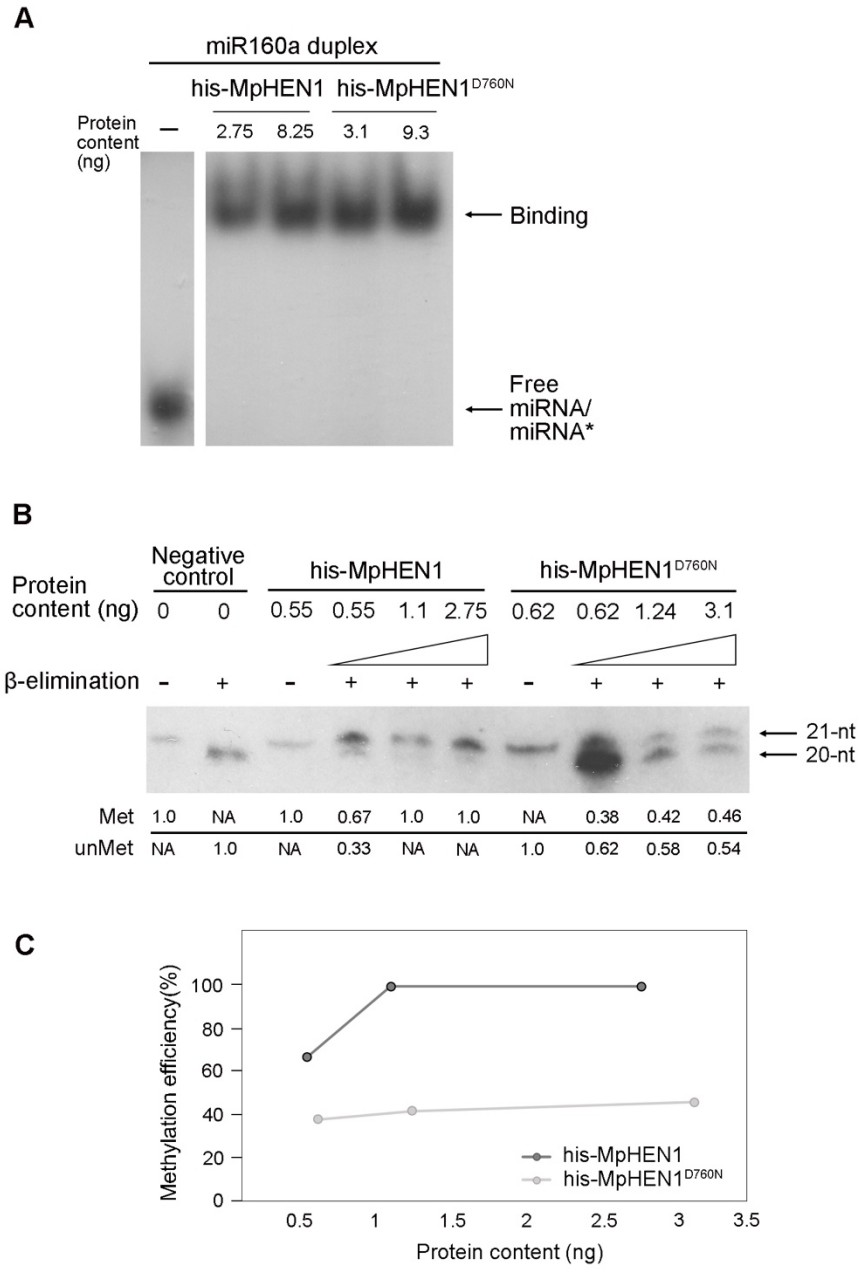

Figure 9. Evaluation of his-MpHEN1 and his-MpHEN1^{D760N} binding small RNAs capability and methylation activity *in vitro*. (A) EMSA for his-MpHEN1 and his-MpHEN1^{D760N} binding to miR160a duplexes. The 0.4 ng of radioisotope-labeled double-stranded synthetic miR160a was used a negative control. (B) The methyltransferase activity of his-MpHEN1 and his-MpHEN1^{D760N} were treated with β-elimination (+) or without treatment (−). (C) Normalized his-MpHEN1and his-MpHEN1^{D760N} methylation efficiency for miR159 duplex.

doi:10.6342/NTU202503912

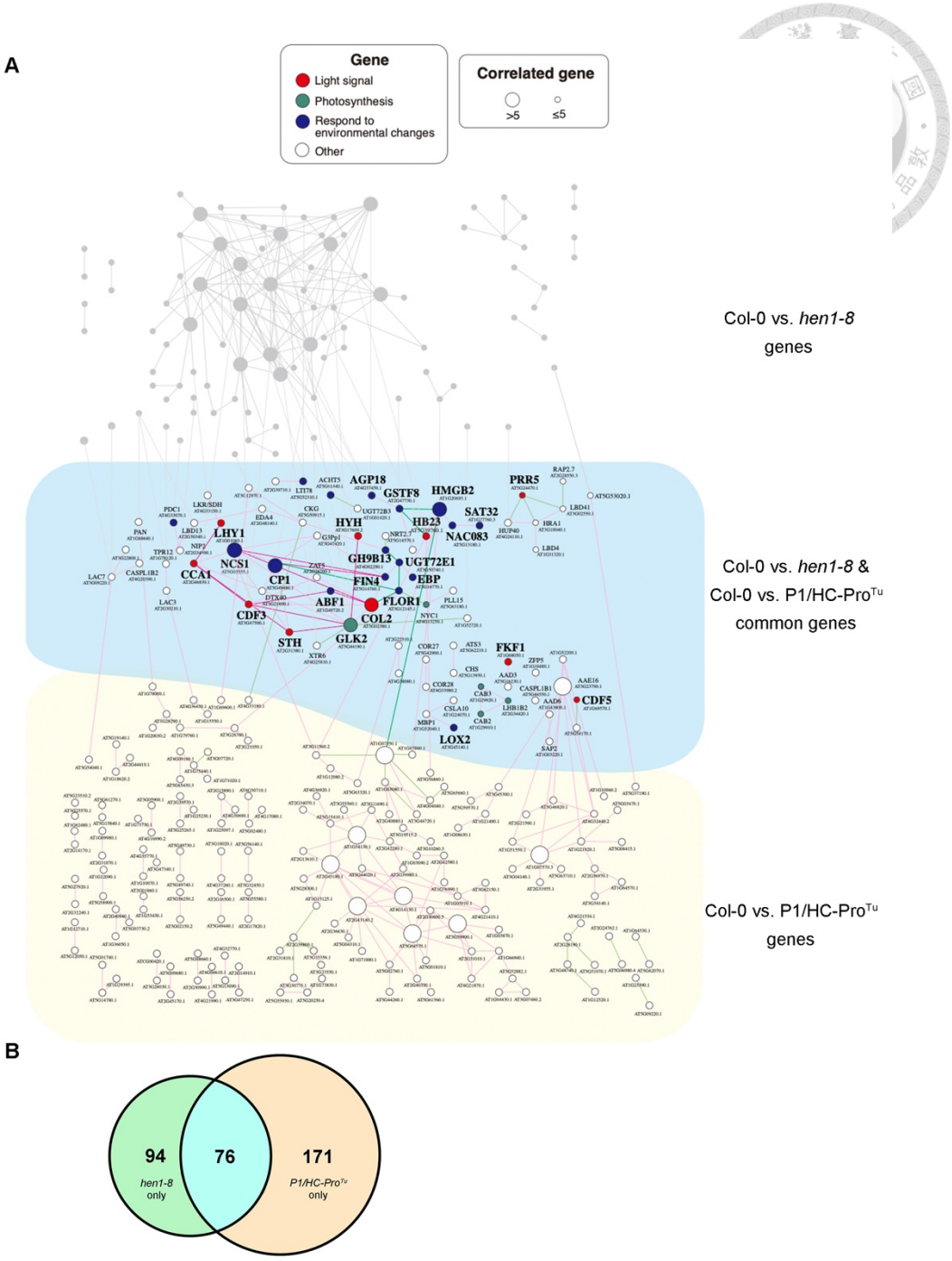

Figure 10. Comparison of gene expression and networks obtained with Col-0 vs. *hen1-8* mutants and Col-0 vs. *P1/HC-Pro*^{Tu} plants (A) The comparative networks Col-0 vs. *hen1-8* mutants and Col-0 vs. *P1/HC-Pro*^{Tu} plants. (B) Venn diagram showing the distributions of shared and unique network genes.

doi:10.6342/NTU202503912

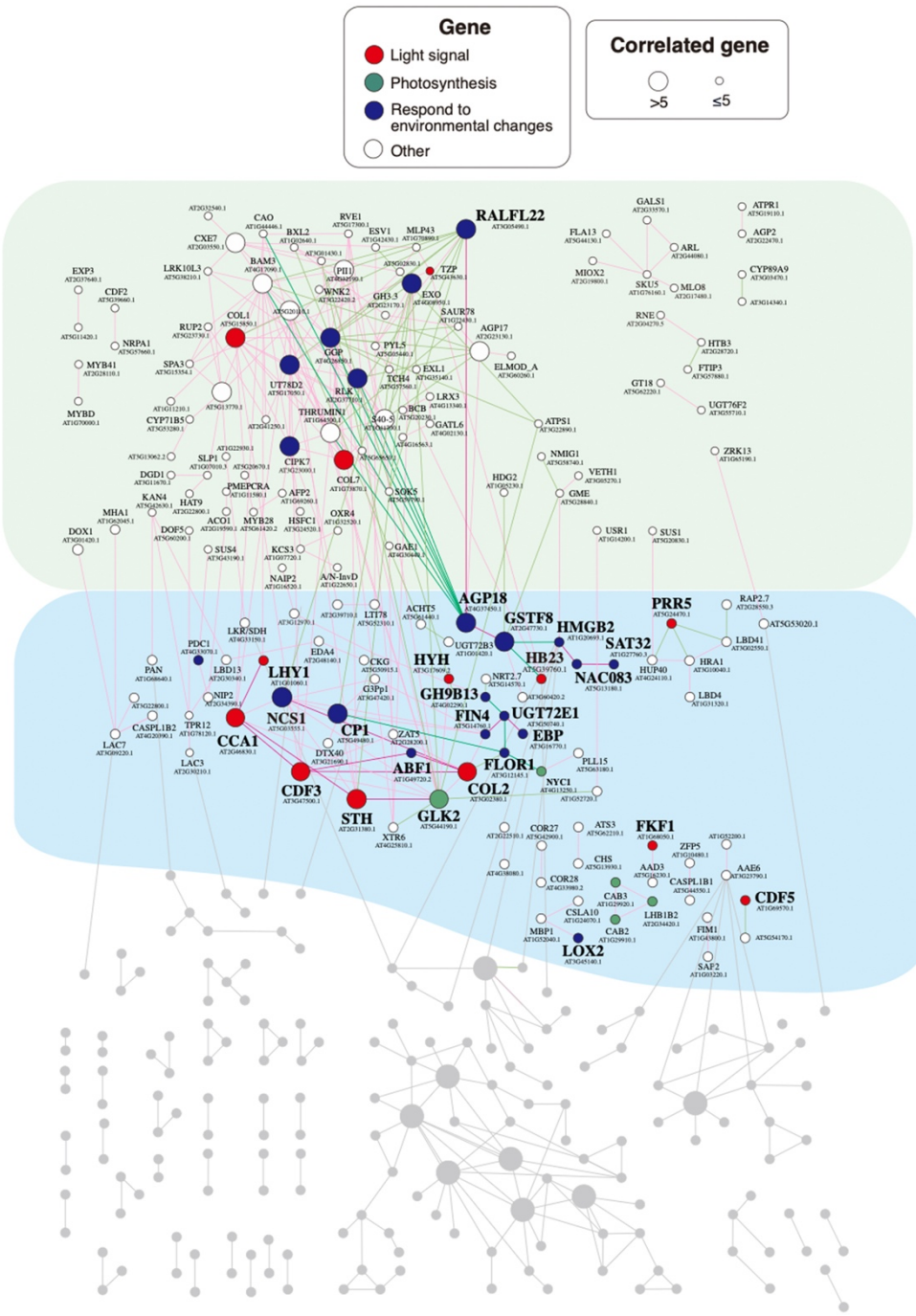

Figure 11. The gene-to-gene network of Col-0 vs. *hen1-8* mutants. A dot represents a gene, a red line represents a positive correlation, and a green line represents a negative correlation. Genes with a green background are unique to *hen1-8*, while genes with a blue background are common to both *hen1-8* mutants and *P1/HC-Pro*^{Tu} plants.

doi:10.6342/NTU202503912

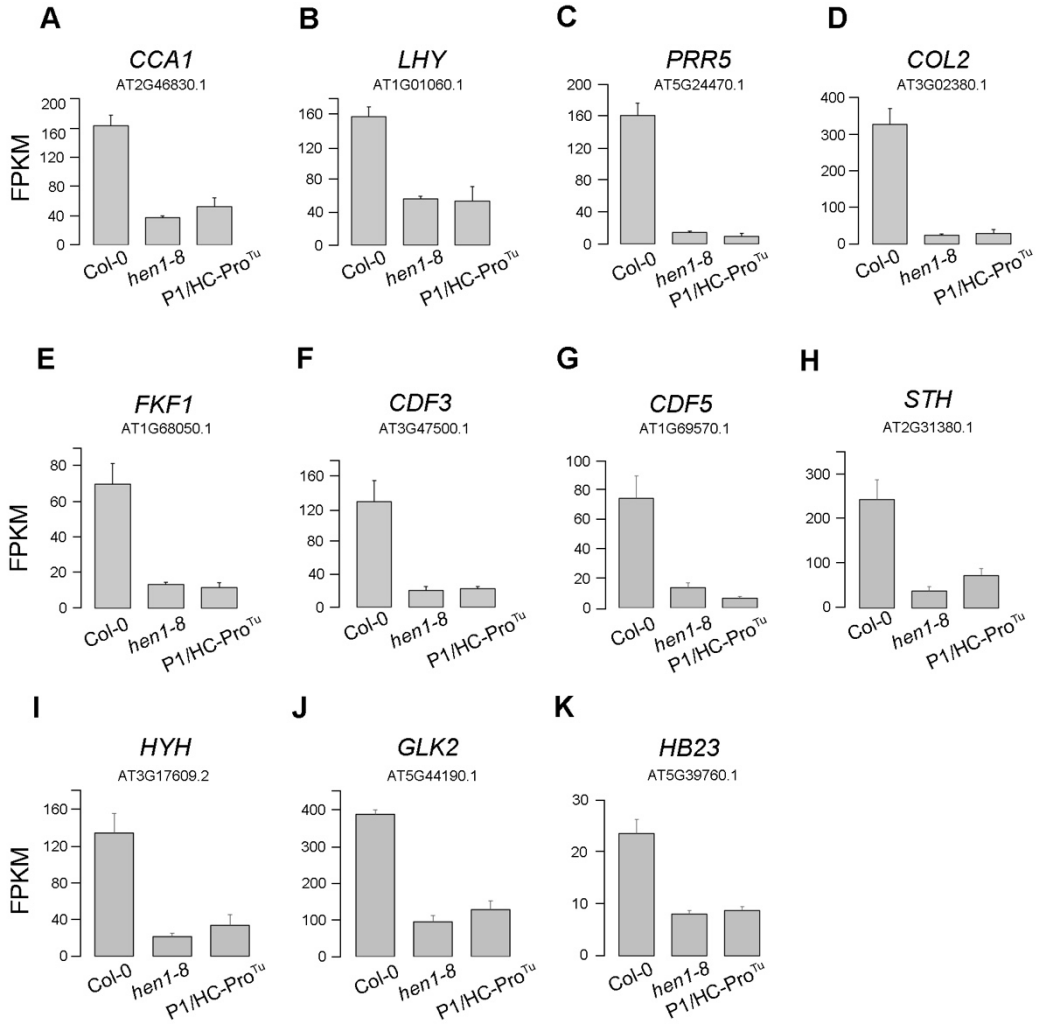

Figure 12. Transcript expression comparisons of light signaling genes in the networks. (A-K) Genes that showed a significant connection, function, or position in the network were selected to demonstrate their transcript expression. The fragments per kilobase of transcript per million (FPKM) were used to represent the normalized transcript expression. The bars represent standard deviations ($n = 3$).

doi:10.6342/NTU202503912

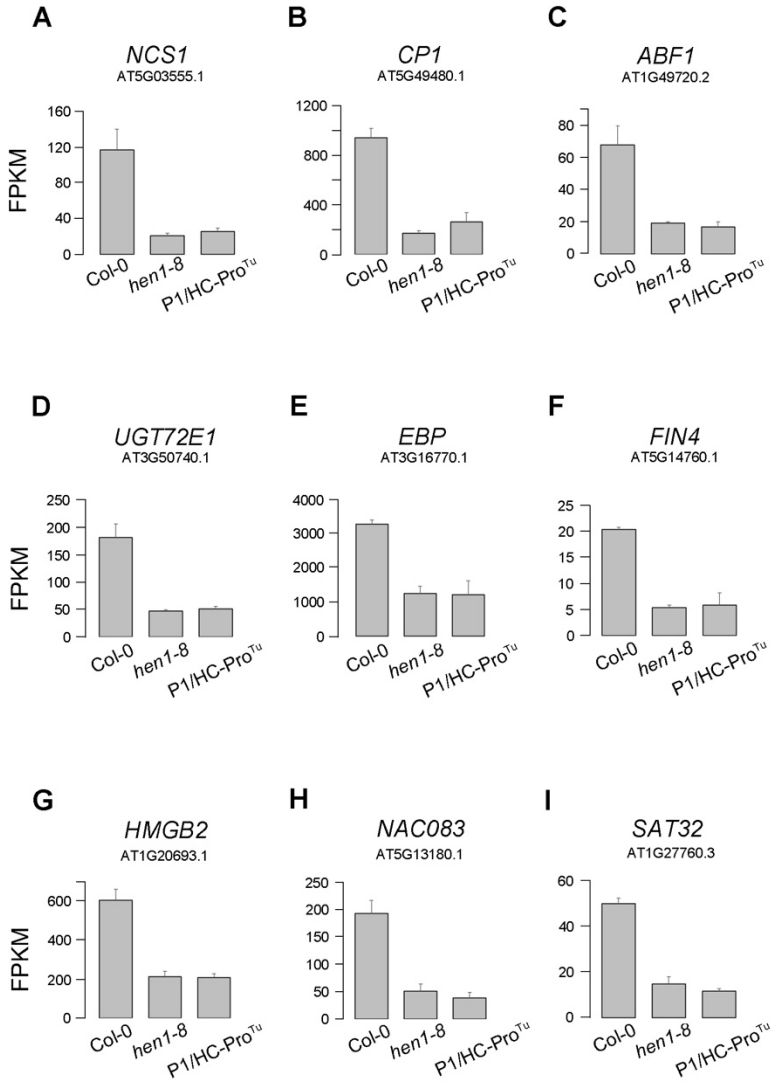

Figure 13. Downregulation of transcript expression in the common genes of *hen1-8* and P1/HC-Pro^{Tu} network. (A-I) Genes showing a response to environmental changes in the network were selected to demonstrate the downregulation of their transcript expression. The fragments per kilobase of transcript per million reads (FPKM) were used to represent the normalized transcript expression. The bars represent standard deviations (*n*=3).

doi:10.6342/NTU202503912

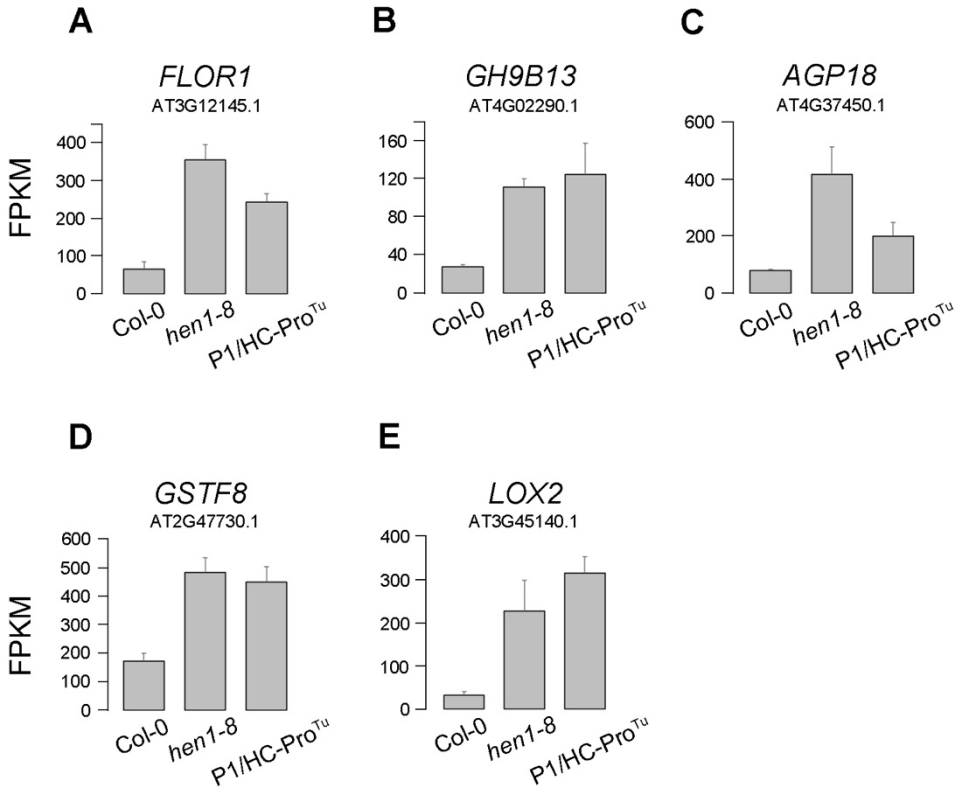

Figure 14. Upregulation of transcript expression in the common genes of *hen1-8* and P1/HC-Pro^{Tu} network. (A-E) Genes showing a response to environmental changes in the network were selected to demonstrate the upregulation of their transcript expression. The fragments per kilobase of transcript per million reads (FPKM) were used to represent the normalized transcript expression. The bars represent standard deviations (*n*=3).

doi:10.6342/NTU202503912

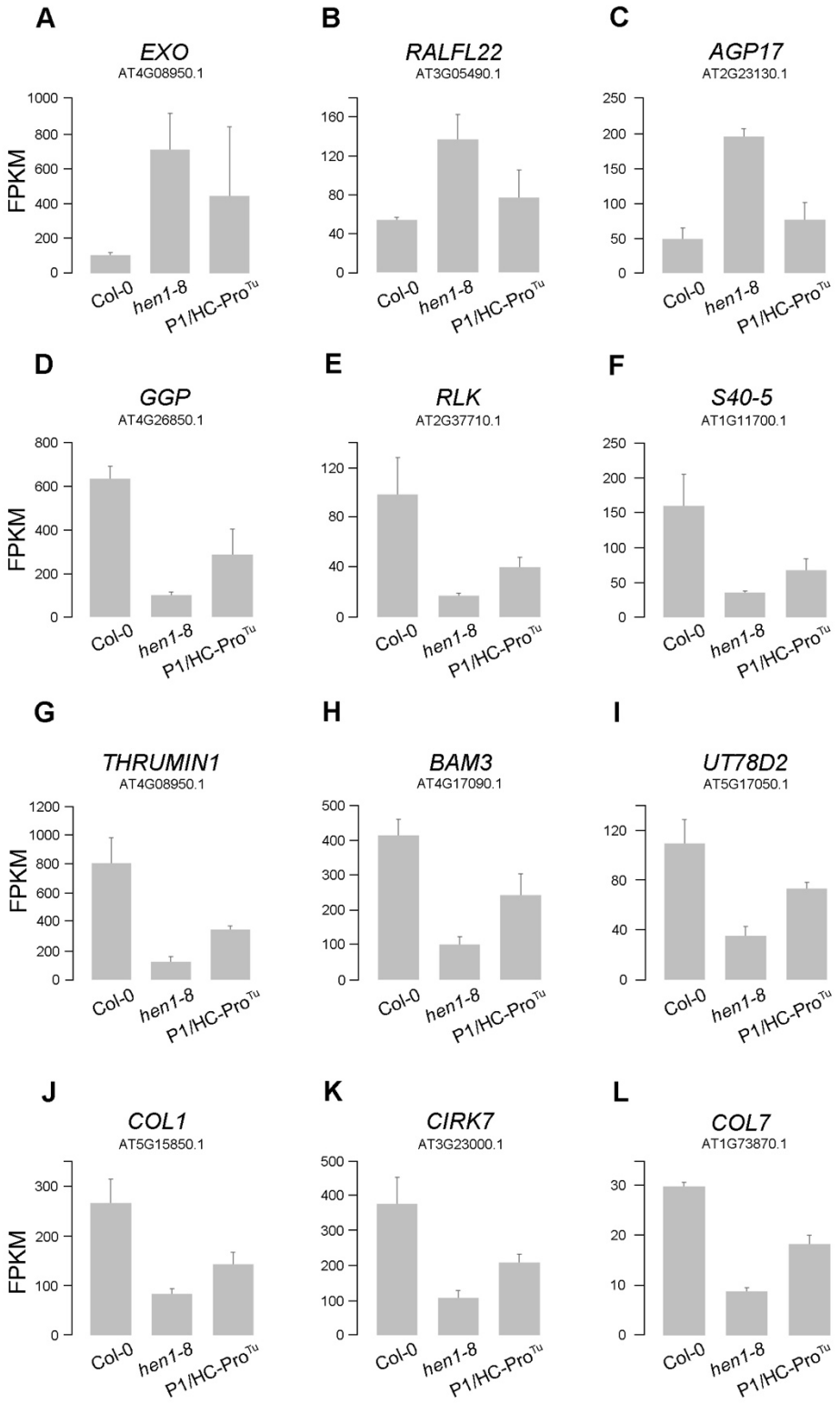

Figure 15. Transcript expression in the unique genes of Col-0 vs *hen1-8* network.

(A-L) The fragments per kilobase of transcript per million reads (FPKM) were used to represent the normalized transcript expression. The bars represent standard deviations (*n*=3).

doi:10.6342/NTU202503912

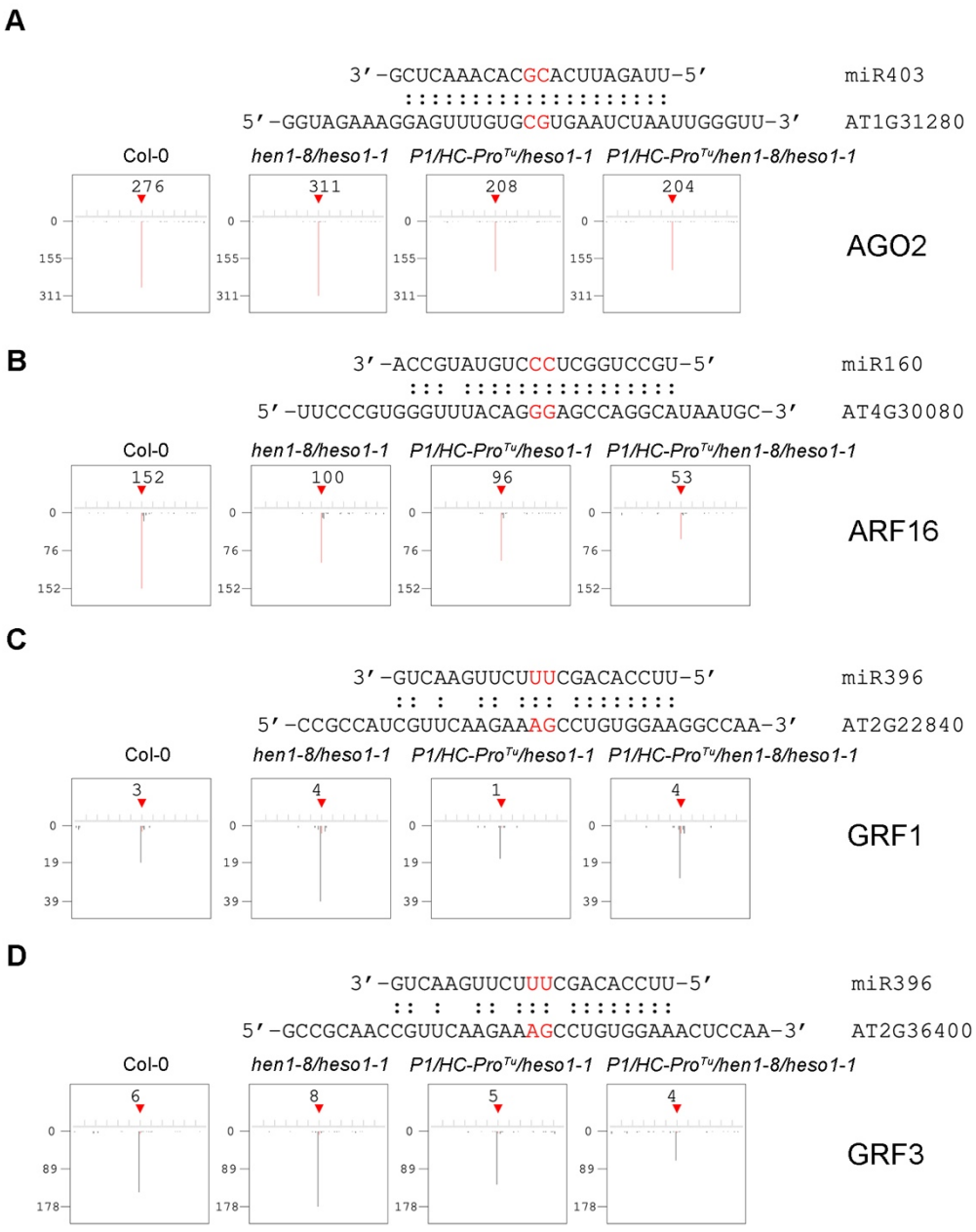

Figure 16. Degradome map of miRNA target *AGO2*, *ARF16*, *GRF1*, and *GRF3* in Col-0 and various mutants. Red triangles indicate the miRNA cleavage position on mRNA. Red lines and numbers indicate the depth of degradome reads.

doi:10.6342/NTU202503912

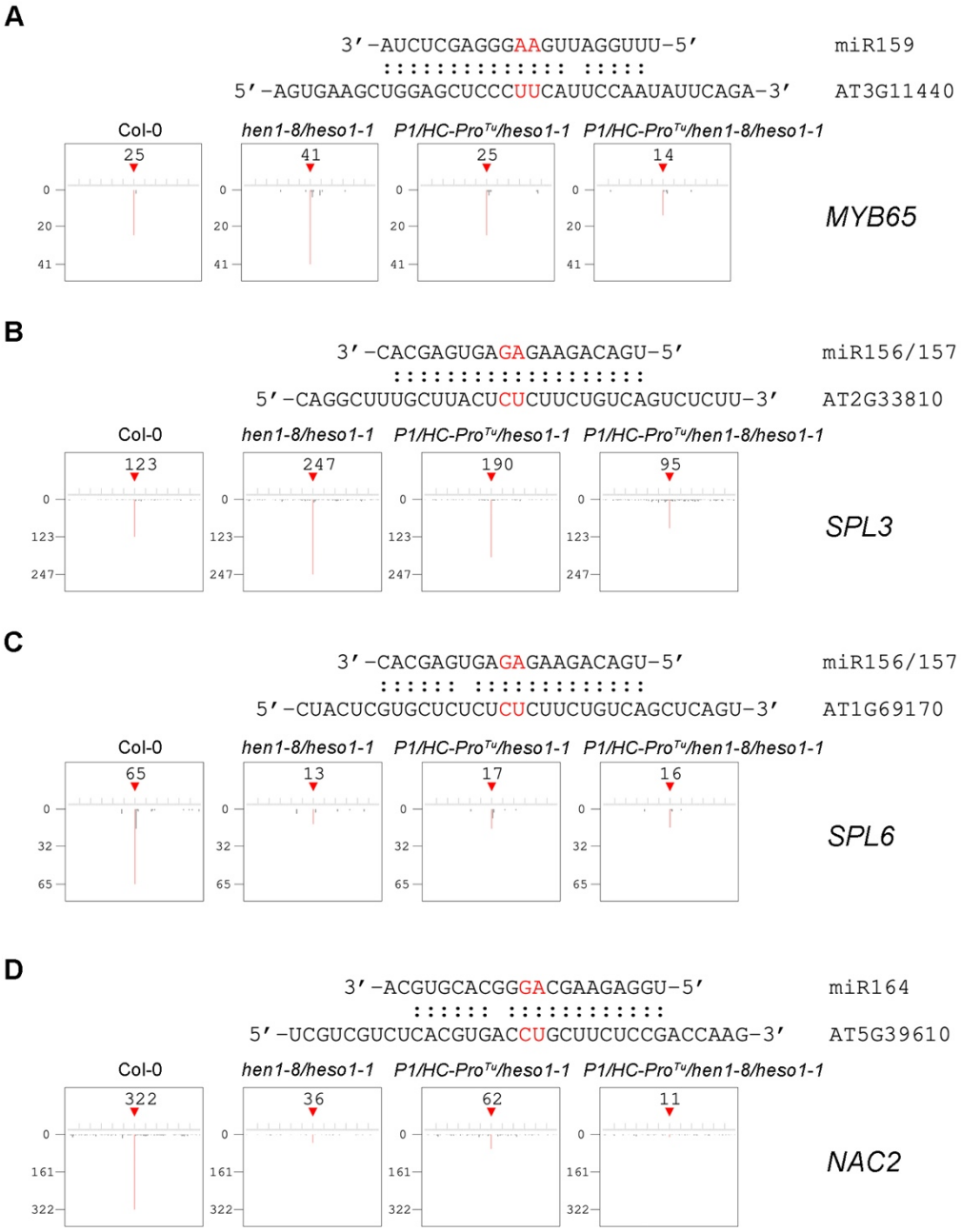

Figure 17. Degradome map of miRNA target *MYB65*, *SPL3*, *SPL6*, and *NAC2* in Col-0 and various mutants. Red triangles indicate the miRNA cleavage position on mRNA. Red lines and numbers indicate the depth of degradome reads.

doi:10.6342/NTU202503912

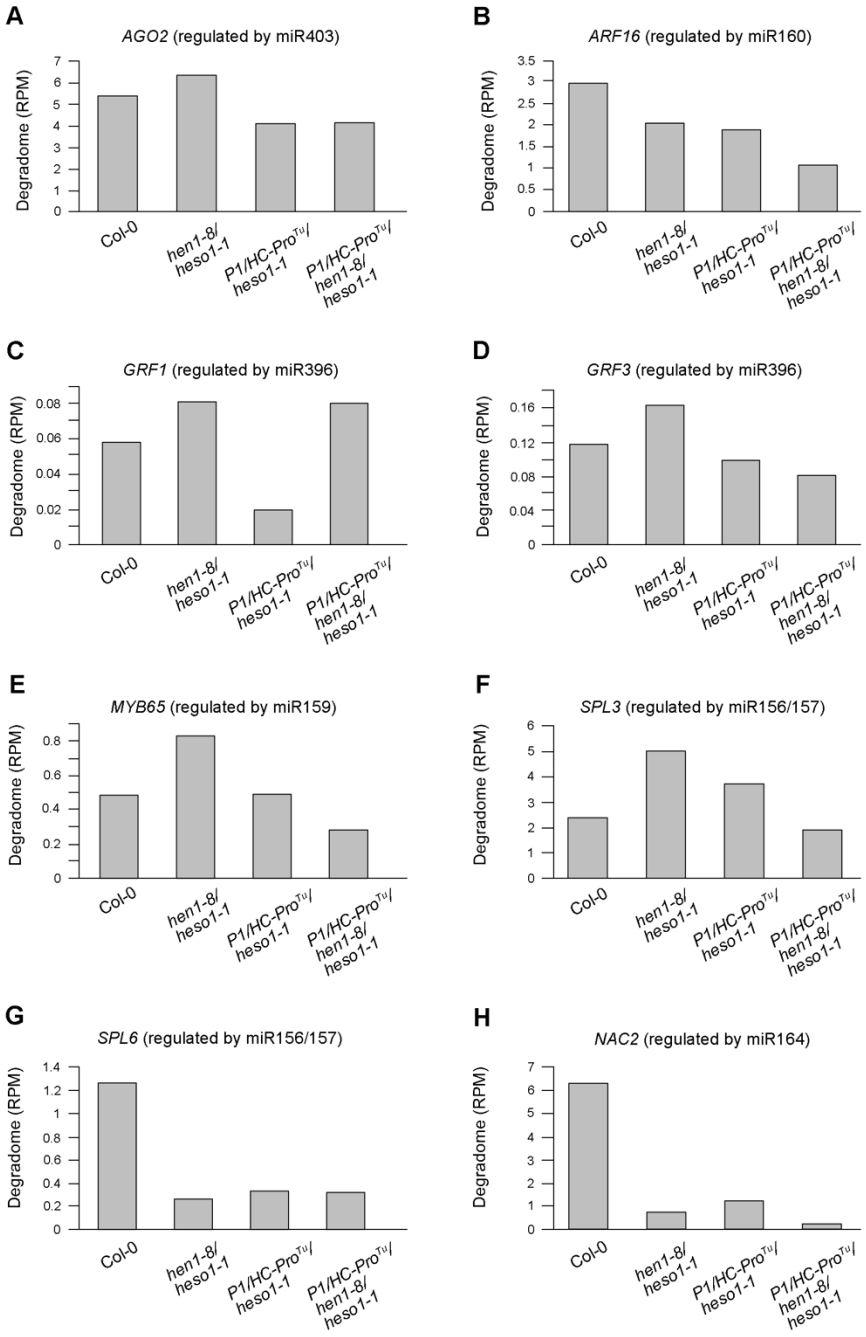

Figure 18. Comparison of RPM mapped reads at the miRNA cleavage position on mRNA between Col-0, *hen1-8/heso1-1*, *P1/HC-Pro^{Tu}/heso1-1*, and *P1/HC-Pro^{Tu}/hen1-8/heso1-1*. The Y-axis represents the RPM mapped reads of the degradome.

doi:10.6342/NTU202503912

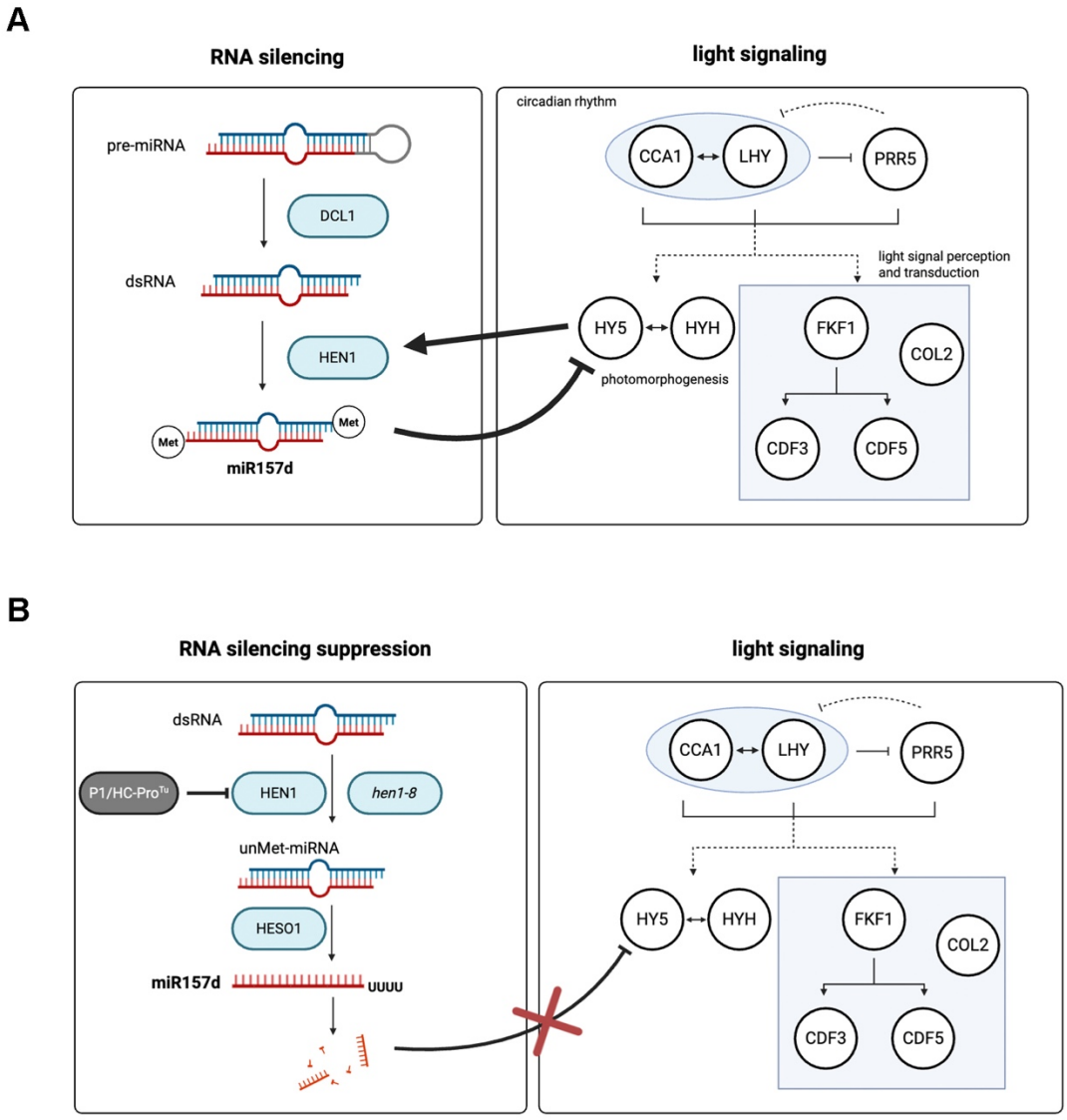

Figure 19. Schematic diagram of the proposed working hypothesis. (A) HY5 and HYH activate the expression of HEN1. HEN1 stabilizes miR157d, which targets the mRNA of HY5 for cleavage, inhibiting the expression of HY5. This forms a negative feedback loop that helps fine-tune the response of photomorphogenesis. (B) When P1/HC-Pro^{Tu} inhibits HEN1 function or HEN1 is inactivated, HEN1 cannot stabilize miR157d, leading to unMet-miR57d being degraded, which cannot suppress the expression of HY5.

doi:10.6342/NTU202503912